Materials Science & Engineering C 89 (2018) 429–443

Contents lists available at ScienceDirect

Materials Science & Engineering C

journal homepage: www.elsevier.com/locate/msec

Antimicrobial and anticancer activities of silver nanoparticles synthesized from the root hair extract of *Phoenix dactylifera*

Mohammad Oves[a,*], Mohammad Aslam[a], Mohd Ahmar Rauf[b], Shariq Qayyum[b], Huda A. Qari[a,c], Mohd Shahnawaz Khan[d], Mohammad Zubair Alam[e], Shams Tabrez[e], Arivalagan Pugazhendhi[f], Iqbal M.I. Ismail[a,g]

[a] Center of Excellence in Environmental Studies, King Abdulaziz University, Jeddah, Makkah 21589, Saudi Arabia
[b] Interdisciplinary Biotechnology Unit, Aligarh Muslim University, Aligarh 202002, India
[c] Department of Biological Science, King Abdulaziz University, Jeddah, Makkah 21589, Saudi Arabia
[d] Protein Research Chair, Department of Biochemistry, King Saud University, Riyadh 11451, Saudi Arabia
[e] King Fahd Medical Research Center, King Abdulaziz University, Jeddah, Makkah 21589, Saudi Arabia
[f] Innovative Green Product Synthesis and Renewable Environment Development Research Group, Faculty of Environment and Labour Safety, Ton Duc Thang University, Ho Chi Minh City, Viet Nam
[g] Department of Chemistry, King Abdulaziz University, Jeddah, Makkah 21589, Saudi Arabia

ARTICLE INFO

Keywords:
AgNPs
Antimicrobial
Biogenic
Candida albicans
E. coli
MCF7
Phoenix dactylifera
Root hair

ABSTRACT

There is a continuous rise in the rate of medicine consumption because of the development of drug resistance by microbial pathogens. In the last one decade, silver nanoparticles (AgNPs) have become a remarkable choice for the development of new drugs due to their excellent broad-spectrum antimicrobial activity. In the current piece of work, we have synthesized AgNPs from the root extract of *Phoenix dactylifera* to test their antimicrobial and anti-cancer potential. UV–visible spectra showed the surface plasmon resonance peak at 420 nm λ_{max} corresponding to the formation of silver nanoparticles, FTIR spectra further confirmed the involvement of biological moieties in AgNPs synthesis. Moreover, XRD analysis showed the crystalline nature of AgNPs and predicted the crystallite size of 15 to 40 nm. Electron microscopy analyses confirmed their spherical shape. In addition, synthesized AgNPs was also found to control the growth of *C. albicans* and *E. coli* on solid nutrient medium with 20 and 22 mm zone of inhibition, respectively. The 100% potency at 40 μg/ml AgNPs concentration was observed against *E. coli* and *C. albicans* after 4 h and 48 h incubation respectively. Importantly, AgNPs were also found to decrease the cell viability of MCF7 cell lines in vitro with IC_{50} values of 29.6 μg/ml and could act as a controlling agent of human breast cancer. Based on our results, we conclude that biologically synthesized AgNPs exhibited multifunctional properties and could be used against human cancer and other infectious diseases.

1. Introduction

Biological synthesis of silver nanoparticles (AgNPs) has great potential because of its use in disinfective medicine and device development [1,2]. On the basis of research and applications, different types, shape, size, and crystalline materials of AgNPs has been synthesized through different physico-chemical methods. However, these physico-chemical methods are expensive, time and energy consuming and also generate huge chemical byproducts [3,4]. On the other hand, green synthesis route of AgNPs is natural, economical and environmentally safe process [5,6]. Several researchers have lucratively synthesized AgNPs by using bacterial, fungal and plant enzymes [7,8]. Among these, plant extract or active compounds are the more promising source for the AgNPs synthesis than bacterial and chemical methods because of no risk of bacterial and hazardous chemical contamination and less energy consumption with greater applicability and simplicity. Currently, many plant species based bio-constituents are used as an innovative eco-friendly and economical utensil to synthesize stable and potential colloidal AgNPs homogenous solutions with monodisperse phase. AgNPs have been synthesized from plant leaves of *Acalypha indica* [9], *Ficus benghalensis* [10], and mulberry [11], and seed extract of *Macrotyloma uniflorum* [12], *Jatropha curcas* [13], *Illicium verum* [14] and *Pistacia atlantica* [15].The AgNPs have also been synthesized from plant roots of *Trianthema decandra* [16] and *Ocimum sanctum* [17], but reports are scarce in comparison to those with leaf and seed extract.

Phoenix dactylifera (date palm) is an important crop in arid and

* Corresponding author at: Building # 4, First floor, CEES, King Abdulaziz University, Jeddah 21589, Saudi Arabia.
E-mail address: mmateenuddin@kau.edu.sa (M. Oves).

https://doi.org/10.1016/j.msec.2018.03.035
Received 21 August 2017; Received in revised form 13 March 2018; Accepted 30 March 2018
Available online 04 April 2018
0928-4931/

Table 1
Table of merit previous and this antimicrobial research works belongs to the synthesis of AgNPs from different plant organs of Phoenix dactylifera

Plant organ	Size (nm)	Dose (μg/ml)	Potency (%)	Antimicrobial and anticancer studies against			Ref.
				Bacteria	Fungi	Cell line	
Fruits	25–60	30	100	*B. cereus* *S. epidermidis* *K. pneumoniae* *E. coli*	ND	ND	[19]
Fruit pit	40	25	83	*K. pneumonia* *A. baumannii*	*R. solani*	ND	[20]
Leaves	26.3	64	100	*E. coli* *K. pneumoniae*	ND	ND	[21]
Root hairs	15–41	20	100	*E. coli*			This study
		20	100		*C. albicans*		
		29.6	IC_{50}			*MCF-7*	
		> 100				*PBMC*	
		> 256				*RBC*	

Notes: Abbreviations: B, *Bacillus*; AgNPs, silver nanoparticles; K, *Klebsiella*; E, *Escherichia*, A, *Acinetobacter*; R, *Rhizoctonia*; S, *Staphylococcus*; OD, optical density; C, *Candida*; MCF-7, Michigan Cancer Foundation-7; HEPES, 4-(2-hydroxyethyl)-1-piperazineethanesulfonic acid; SEM, scanning electron microscopy; TEM, transmission electron microscopy; EDX, energy dispersive X-ray; FTIR, Fourier transform infra-red.

semiarid regions of the world. It has a main role in the social lives and economy of gulf countries, including Saudi Arabia, UAE, and Iran. *P. dactylifera* plant has root fibers cover stem above the ground. To our knowledge, the collection of the root fibers from the stem above the ground does not affect the plant health and considered as a solid waste and inexpensive material. Upon careful exploration, *P. dactylifera* leaves, fruits, seeds and bark contain antimicrobial activity and the synthesis of silver nanoparticles have been reported in the literature, but the synthesis from the root fibers are still unexplored [18]. *P. dactylifera* fruits, leaves, and seed mediated silver nanoparticles have been synthesized for antimicrobial activity [19–21] (Table 1). Root fibers extracts have antimicrobial activity and has reported to change the oxidation state of silver ion from Ag^+ to Ag^0 and act as a synthesizing agent for AgNPs without the involvement of reducing chemical agents in the reaction mixture. AgNPs synthesized from aqueous extracts of plant root hair, novel properties because of the presence of different bioactive compounds such as polyphenols, lipids, and fatty acids. The involvement of these bioactive compounds in synthesis of AgNPs helps to maintain specific characteristics such as size, distribution, morphology of the materials and their application. Normally nano range particles show a higher surface area-to volume ratio. The specific surface area is relevant for catalytic activity such as antimicrobial activity of nanoparticles [9,10]. As the specific surface area of nanoparticles is increased, their biological effectiveness can also increase on the account of a rise in surface energy.

Historically, silver is extensively used as a potent therapeutic agent [22]. Biologically synthesized AgNPs are reported for the antimicrobial and anticancer activities [23,24]. Recently, there was a surge in the application of nanomaterials for the development of diagnostic tools like bio-sensing, bio-imaging, and many others. Nanoparticles application in the clinical imaging modalities could affect the biological factors in the microenvironment and recognizes prior change and smaller growth stage of tumor or cancer cells [25]. Bio-inorganic materials have the ability to significantly interact with cells and its complements. It can also easily uptake by the membrane and lead to the generation of reactive oxygen species, which incite the oxidative stress [26]. It is well known that synthesized AgNPs induces cell damage through the loss of cell membrane integrity, oxidative stress and apoptosis [27]. AgNPs treated MCF-7 cells showed a clear effect on the alteration in cell shape apparent to morphological variations, for example, coiling and cell shrinkage compared to control cells [28,29]. Interestingly, the use of biogenic AgNPs for the diagnosis of cancer leads to the emission of bright red fluoresce inside the cancerous cell [30]. Recently, researchers have experimentally confirmed the nontoxic and biocompatible nature of AgNPs [31].

Candida albicans belongs to the dimorphic fungi and cause 90% candidacy in mammals and humans [32,33]. It is commonly colonizes and grow on mucous membrane of the mouth, tongue, and vagina [34]. It also causes systematic fungal infection in immune-compromised patients suffering from AIDS, cancer and organ transplantation. *C. albicans* can grow in the form of a biofilm on the surface of medical devices and surgical instruments. It is also causing nosocomial infection and approximate 90% vaginal infection every year [35]. In addition, their long term infection develops overgrowth and develops resistance to antifungal drugs [36]. *Escherichia coli* is a major organism of nosocomial and water borne infection with higher morbidity and mortality rates is the other organism used in this study [36]. Both organisms adapt through different mechanisms to develop resistance against multiple drugs. However, antimicrobial activity of biogenic silver nanoparticles is common while particles formation and purification is not monitoring the actual value of the developed AgNPs. Most of these studies used conventional propensity methods for testing bacterial growth inhibition such as agar diffusion test to measure bacterial zone of inhibition by AgNPs and minimal inhibitory concentration (MIC) and minimal bactericidal concentration (MBC). However, only a few researchers used standardized techniques like diffusion and dilution for determining MIC of green synthesized nanoparticles. To the best of our knowledge, there is no concentrate study to evaluate the antimicrobial potency of biogenically synthesized AgNPs using standard bacterial growth kinetic study. Consequently, the aim of the current study was to analysis the dose dependent activity and potency of newly synthesized AgNPs from *P. dactylifera* root hair aqueous extract against *E. coli* and *C. albicans*. In addition, we have also investigated newly synthesized AgNP effect on human breast cancer cell line MCF7, Peripheral blood mononuclear cells (PBMCs) and RBC lysis in vitro condition. Further apoptotic potential of AgNPs was confirmed by dual AO/EtBr staining and cell cycle analysis.

2. Material and methods

2.1. Chemicals and reagents

Analytical grade silver nitrate ($AgNO_3$) was purchased from the La Pine scientific company (Chicago USA). Culture media, peptone broth and nutrient broth were obtained from Scharlau Chemie S.A. (Barcelona, Spain). Human breast cancer cell line MCF7 was procured from the American Type Culture Collection (ATCC, Rockville, Maryland, USA). Dulbecco's modified eagle medium (DMEM) was purchased from the UFC Biotech Company, (KSA) whereas tissue culture plastic wares were obtained from BD Biosciences (USA). Fetal

bovine serum, 2-propanol, penicillin, streptomycin and 3-[4,5-dimethylthiazol-2-yl]-2,5-diphenyl tetrazoliumbromide were purchased from Sigma Chemical Co. (St. Louis, MO, USA).

2.2. Phoenix dactylifera root fiber collection and extract preparation

Tribal *Phoenix dactylifera* root fibers were collected from the young plant of orchard of King Abdulaziz University Campus Jeddah, KSA. The root fibers were removed by knife and washed three times with distilled water and two times with 70% ethanol. Washed fibers were dried at 80 °C in oven (JSOF-100H, JS Research Inc. Korea) and grind into a fine powder using 80 mm mesh size grinder (FOSS cyclotec 1093, Sweden). The amount of 1 g powdered was transferred in 250 ml flask containing 100 ml deionized water and boiled at 100 °C for 30 min. Cooled and decanted plant root broth solution was passed through 0.25 μm syringe filter to remove particulate materials and stored at 4 °C for further characterization.

2.3. Green synthesis of silver nanoparticles

In this study, the biogenic silver nanoparticles were synthesized by bottom up approach and fallow the slightly modified method of previous studies [37]. In a 250 ml volumetric flask, 95 ml of 0.1 mM aqueous solution of silver nitrate was prepared and 5 ml root fibers extract was added to monitor the reduction of Ag + ions into Ag^0. After 30 min, the color of solution mixture was changed from light yellow to yellowish brown, reddish brown, and finally to colloidal brown. These color changes were monitored by UV–visible spectrophotometer (UV-1800, Shimadzu, Japan). This reaction was performed separately in three sets at various concentrations of both silver nitrate solution and root fiber extract. To avoid photo-activation of $AgNO_3$, the reaction was carried out in the dark at room temperature. Suitable controls were maintained throughout the condition of experiments. Complete reduction of Ag^+ ions was confirmed by the change from colorless to brown color. Colloidal solution was kept at room temperature for 24 h to complete reduction. The colloidal mixture of AgNPs was sealed in glass vials and stored properly at 4 °C for characterization.

2.3.1. Purification of biogenic AgNPs and release kinetics

The *dactylifera* root hair extract was used for the synthesis of AgNPs. The synthesized nanomaterials were washed four times by double distilled water and redispersed method was used to remove the unused silver ions. Further synthesized materials were transferred into HEPES buffer and put into the dialysis bag. The materials containing bag was re-suspended in 10 ml of HEPES buffer (20 mM, pH 7.4) amended with sucrose solution to reach a density of 2.5 g/ml. A 10 ml of a linear gradient of sucrose (0.25–1.0 M) density was layered on the nanoparticle suspension and subjected to centrifugation (10,000 rpm at 5 °C for 2 h) and were collected for further characterization. The concentration of nanoparticle in solution was determined by ICP-AES (Shimadzu, Japan).

Biogenic AgNPs synthesized materials were filled in a dialysis bag (12 kDa, cutoff). These bags were suspended in a buffer solution (HEPES, 50 ml, pH 7.4) for overnight and analyzed the release rate and order of kinetics of AgNPs in liquid medium. The concentration of releasing ions was measured by ICP-AES (Shimadzu, Japan). Concisely, 1 ml solution of AgNPs was mixed with 9 ml of concentrated nitric acid and 3 ml of sulfuric acid for the digestion that converts it into atomic form. Furthermore, the reaction mixture was processed at 100 °C on a hot plate for 2 h for complete salvation. Prepared sample was analyzed in the presence of air/acetylene flame with flow rate 0.9 to 1.2 L/min and atomize temperature 1200 °C. The silver ion released in % was calculated by using an equation

$$\%\text{released of silver ion} = \left[\frac{Wt}{Wc}\right] \times 100 \quad (1)$$

Here, Wt is the released ions in the buffer solution and Wc is the total silver content in the dialysis bag at that time.

2.3.2. Characterization of AgNPs

2.3.2.1. UV–visible spectroscopy. Bio-reduction of silver ion from the prepared colloidal mixture of AgNPs was analyzed by the UV–vis absorption spectra as a function of time and temperature. About 3 ml of brown reaction mixture was used to periodically monitor the complete bioreduction of Ag + in aqueous solution. UV–vis spectra were recorded at 10, 20, 40, 50, 60, 45 and 60 min and till 48 h and separately reaction setup was placed at 10, 20, 30, 40, 50, 100 and 200 °C temperature to achieve optimum efficiency of AgNPs synthesis.

2.3.2.2. FTIR spectroscopy. Synthesized nanomaterial was also analyzed by Fourier transform Infra-red (IRAffinity-1, Shimadzu, Japan) spectra. Samples of AgNPs were prepared with KBr crystal as a beam splitter to determine the involvement of biological moieties in particle synthesis. In order to remove undesirable plant materials and silver, the sample was centrifuged at 10,000 rpm for 10 min and the resulting pellets was dried at 80 °C and grounded with KBr crystal. The FTIR spectra of $AgNO_3$, aqueous date seed extract, and AgNPs were recorded as a KBr pellet at a resolution of 4 cm^{-1} in the wave number region of 400–4000 cm^{-1}.

2.3.2.3. X-ray diffraction (XRD). Crystal analysis was done by X-ray diffraction patterns of fine AgNPs. XRD was carried out using X-pert, X-ray powder diffractometer (Philips PW1398) with Cu-Kα radiations (l = 0.15406 nm) in 2θ range from 20 to 80°.

2.3.2.4. Electron microscopy and energy dispersive X-ray. Biogenic AgNPs were characterized using field emission scanning electron microscopy (FEI, Quanta FEG 450). Samples of the AgNPs were attached to the grid using carbon or copper tape and sputtered with gold by means of sputter coater (Quorum Q150R ES, Quorum Technologies Ltd. Ashford. Kent. England). The voltage was set at 5 kV and 10 kV. The elemental information of the attached sample was observed by energy dispersive X-ray (EDAX) (Amtek GmbH, Wiesbaden, Germany). In addition to this, size and shape of the nanoparticles were also confirmed by transmission electron microscopy (TEM) (JEOL JEM-1011, Japan).

2.3.2.5. Nanophox spectra analysis for particle size. The reduction of silver ions A^+ in to A^0 elemental particle form in the reaction mixture was monitored by UV–Visible spectrum. The reaction mixture was evaluated with the help of the Nanophox particle size analyzer [38]. A 1 ml amount of sample diluted with double distilled water and takes overnight and analyzed the distribution and stability of the sample. A yellowish stable brown color was observed in the presence of nanomaterials. A 3 ml reaction mixture was takes in the cuvette and optimized reading rate of silver ion at a different wavelength. Particle size and size distribution analysis of suspensions was done by Photon Cross-Correlation Spectroscopy (PCCS) (Sympatec GmbH, Germany). Samples (2 ml) were put into cuvette placed in thermostat bath filled with clean water (filtered by 022 μm filter). It has to be orthogonal to the incoming laser beam with 632.8 nm wavelength.

2.4. Antimicrobial activity

2.4.1. Zone inhibition assay

Antimicrobial activity of synthesized AgNPs was performed against *E. coli* and *C. albicans* strains. These microbial cultures were collected from the medical center of King Abdulaziz University. The fungi and bacterial strains were inoculated in 2% peptone broth and 1.4% nutrient broth, respectively, and placed overnight at 35 °C in an incubator to obtain a fresh culture. Growth inhibition assays were performed in both liquid and solid agar plate medium by the diffusion method, modified from Bauer et al. [39]. A 100 μl amount of fresh culture from

each microbial strain were inoculated into 10 ml of sterile nutrient and peptone broth separately and incubate and standardize the culture according to McFarland standards (10^6 CFU ml^{-1}). (According to the McFarland standard, fix the correlation between optical density reading and colony forming unit (CFU). McFarland standard are used as a reference to monitor the bacterial count in the suspensions during standardize microbial testing. It made from the specified concentration of barium chloride and sulfuric acid.) These fresh cultures of bacteria and fungi (100 μl) were spread on nutrient agar and Czapk media plates for optimum growth, respectively. All of the plates absorbed the culture and 8 mm size bore was made at different locations and then sealed with sterile molten agar to prevent the inside leakage of testing materials and standard drug. On each plate well, 100 μl suspensions of AgNPs and root extract as a negative control, were loaded and incubated overnight at 37 °C. Fluconazole and amoxicillin were used as a positive control in case of fungal and bacterial strains respectively.

2.4.2. Growth kinetic and interfacial interaction study

The biogenic AgNPs interfacial and interfacial interaction to the cell surface was approved by growth kinetic study. *E. coli* and *C. albicans* survival rate was measured in the presence or absence of different dose of green-synthesized AgNPs. For this investigation bacterial and fungal cells *E. coli* and *C. albicans* were grown in nutrient broth and peptone broth containing flask, respectively. Further these flasks were incubated overnight on a shaker incubator at 35 °C and 125 rpm. Freshly prepared 100 μl cultures were transferred into sterilized 100 ml nutrient broth and peptone broth containing flasks. After 1 h of inoculation (approximately initial stage of log phase), different amount of AgNPs doses (0, 5, 10, 20, 40, 80 and 100 μg/ml) was amended in actively growing organisms of *E. coli* and *C. albicans* culture containing flasks. Further these, treated culture was withdrawing (3 ml) every hour and optical density was recorded at 600 nm by UV–visible spectrophotometer (Shimadzu, UV1800-240V, Kyoto, Japan). All these experiments were carried out in triplicates.

2.4.3. Potency of biosynthesized AgNPs

The efficiency of green synthesized AgNPs on growth inhibition of *E. coli* and *C. albicans* were investigated. During incubation with AgNPs at the end of every hour, (1 ml culture) sample was withdrawn from each culture tube and transferred to a sterile test tube. A series of serial dilution prepared up to 5-fold with sterile saline water for the spread plate count method on sterile nutrient agar and potato dextrose agar plates. From each dilution three plates were prepared and incubated for overnight at 35 °C. The next day colonies on some plates were counted by using colony counter (Colony Count V, Gerber Instruments AG, Effretikon, Switzerland). The effect of AgNPs on the growth of microorganisms was compared with control and the potency of AgNPs was observed by using below mentioned Eq. (2).

$$\text{Potency of AgNPs}(\%) = \frac{[(\text{cfu/ml})_{control} - (\text{cfu/ml})_{treated}]}{(\text{cfu/ml})_{control}} \times 100 \quad (2)$$

2.4.4. Effect of AgNPs on surface cell surface morphology

The organisms *E. coli* and *C. albicans* cell surface morphology was demonstrated by field emission scanning electron microscopy with EDAX (FEI, Quanta FEG 450). For this purpose the AgNPs treated and positive control samples 1 ml cultures were withdrawn and taken in eppendorfs and centrifuged at 5000 rpm for 10 min to find the cells in the form of pellets. The cells containing pellets were washed three times with phosphate saline buffer. Further, washed cells of *E. coli* and *C. albicans* was fixed with the 2.5% glutaraldehyde solution and incubated for overnight at 4 °C. Furthermore, 100 μl of fixed sample was washed three times with sterilized distilled water and centrifuged 1000 rpm, cell pellets were mixed with 100 ml Milli Q water and spread on a glass slide. These glass slides were taken in 1% tannic acids for 10 min and washed two times with 50% and 70% ethanol. After fixation glass slides were splattered with gold coating by sputter coater (Quorum Q150R ES, Quorum Technologies Ltd. Ashford, Kent, England) and analyzed in FESEM.

2.4.5. In vitro erythrocyte lysis test

An in vitro RBC lysis test was performed in order to study the toxicity of synthesized AgNPs, by assessing the hemoglobin released as a result of membrane leakage or disruption caused by exposure to different doses of the nanoparticles. Briefly, fresh blood from a healthy rabbit was collected in an anticoagulant solution (EDTA) followed by centrifugation at 1200*g* (10 min, 4 °C) and the buffy coat and plasma were discarded. Washed erythrocytes were diluted with isotonic buffer (20 mM PBS) to prepare 50% hematocrit. The extent of hemolysis was analyzed by incubating the RBC suspension with varying concentrations of the synthesized AgNPs (37 °C, 1 h). The incubated solutions were centrifuged at 1500*g* for 10 min and the supernatant was collected and λ_{max} was read at 576 nm in the UV–visible spectrometer to find out released hemoglobin. The percentage hemolysis was calculated by the below-mentioned equation Eq. (3) [40]:

$$\text{Hemolysis}(\%) = \left(\frac{\{Abs_T - Abs_C\}}{Abs_{100\%}}\right) \times 100 \quad (3)$$

where Abs_T is the absorbance of the supernatant from samples incubated with different AgNPs concentrations, Abs_C is the absorbance of the supernatant from controls (normal saline), and $Abs_{100\%}$ is the absorbance of the supernatant of controls exposed to 1% Triton® X-100, that causes complete lysis of RBCs.

2.4.6. Anticancer activity of AgNPs

To evaluate the anticancer potential activity of AgNPs, both breast cancer cell lines (MCF-7 cells) and peripheral blood mononuclear cells (PBMCs) were employed as a control. MCF-7 and PBMCs were kindly provided by the King Fahd Medical Research Center, King Abdulaziz University, Saudi Arabia. The cells were cultured in DMEM supplemented with 10% FBS at 37 °C under a humidified atmosphere containing 5% carbon dioxide. After attainment of 70% confluency, the cells were trypsinized with a buffered saline solution containing 0.25% trypsin and 0.03% EDTA. Subsequently, the cells were plated to the culture plate as desired and allowed to attach for 24 h.

2.4.6.1. MTT assay. To assess cell viability of the treated cells MTT assay was performed. MTT (Thiazolyl Blue Tetrazolium Bromide), is a yellow dye which gets converted into formazan, by the activity of the mitochondrial dehydrogenase enzyme. Briefly, 10^4 cells per well were seeded in 96 well plate and allowed to adhere overnight for both cells. Next morning, the medium was aspirated and the cells were incubated at 37 °C for 24 h with varying concentration of AgNPs and for 4 h with MTT dye (5 mg/ml in PBS). The reaction mixture was aspirated and the resulting formazan crystals were dissolved by adding 200 μl of DMSO. After 10 min, absorbance was read at 490 nm on a Genetix580 microplate reader (USA). Untreated sets served as control which was performed simultaneously under identical conditions. Finally, OD values of culture were converted into a percentage viability by using the following Eq. (4) [41,42]:

$$\text{Cell viability}(\%) = \left[\frac{OD_{Sample}}{OD_{Control}}\right] \times 100 \quad (4)$$

2.4.6.2. Apoptosis assay by acridine orange/ethidium bromide staining. MCF-7 cells were treated with 15 and 30 μg/ml AgNPs for variable time periods. An aliquot (100 μl) of treated cells (~1.25×10^6/ml) was incubated with 1 μl of acridine orange/ethidium bromide (one part each of 100 μg/ml acridine orange and 100 μg/ml ethidium bromide in PBS) just prior to microscopy. A 10 μl aliquot of the gently mixed suspension was placed on microscope slides,

covered with glass slips, and examined under a Zeiss microscope connected to a digital imaging system. Acridine orange is a vital dye that stains both live and dead cells, whereas ethidium bromide stain only those cells that have lost their membrane integrity. Live cells stain uniformly green and can be distinguished from apoptotic cells as they exhibit yellow to orange coloration depending on the degree of loss of membrane integrity due to co-staining with ethidium bromide [43].

2.4.7. Cell cycle analysis

The cell cycle analysis was performed following published protocol with slight modification [44]. Briefly, MCF-7 cells (60% confluency) were treated with synthesized AgNPs for 24 h at varying concentrations of 15 and 30 μg/ml. After the treatment, cells were processed and incubated in 0.5 ml of saponin/propidium iodide (PI) solution (0.3% saponin [w/v], 25 μg/ml PI [w/v], 0.1 mM EDTA, and 10 μg/ml RNase [w/v] in PBS) at 4 °C for 24 h in the dark. Cell distribution was evaluated using Cell Quest software in a FACS Calibur (Becton Dickinson, USA) at the central instrumentation facility of Jawaharlal Nehru University, New Delhi, India for 10,000 events per sample after appropriate gating to determine the percentage of cells in each phase of the cell cycle.

3. Results

3.1. Characterization of nanomaterials

3.1.1. UV–vis spectra analysis of green synthesized nanoparticles

Biogenic synthesis of AgNPs was carried out by the reduction of Ag^+ to Ag^0 in $AgNO_3$ solution through the aqueous root hair extract at optimum temperature. In the reaction mixture just after 30 min, development of light to dark brown color appears which is an indicative of the reduction of silver ion in elemental form and was confirmed by maximum absorption peak observed between 418 and 420 nm (Fig. 1a). We have also investigated the effect of time and temperature on the AgNPs (Fig. 2) productivity and production efficiency. For this purpose, we optimized the concentration of $AgNO_3$, volume of date root extract 1% and time of incubation at optimum temperature at 50 °C. The UV–Visible spectra were recorded from date root hair extract at different reaction times from 10 min to 48 h (Fig. 1b). We found that the formation of AgNPs started after 10 min of incubation and reaction was successfully completed within 48 h further stability check after 30 days. The spectrum indicates the presence of a strong SPR curve between 415 and 425 nm with peak centered at 420 nm (Fig. 1a). Moreover, UV–vis spectra indicate an increase in the absorbance intensity of the reaction mixture with time (Fig. 1b), however, after 48 h no further increase in SPR was observed. These observations indicate that an increased

Fig. 2. During biogenic AgNPs preparation, maximum yield of 79% was optimized at 1% plant root extract with 0.1 molar $AgNO_3$ solution mixture after 48 h incubation at 50 °C temperature.

number of AgNPs was synthesized in the mixture with time and after 48 h no further increase in formation of nanomaterials occurred, which indicates the completion of reaction in the solution and the solution was found to be stable up to 30 days. To study the effect of temperature, we synthesized AgNPs at various temperature; 10, 20, 30, 40, 50, 100 and 200 °C. The UV–vis spectra results indicated that AgNPs synthesis using date root hair extract was increased at elevated temperature on a similar wavelength at 420 nm (Fig. 1).

3.1.2. Purification and release kinetics of biogenic AgNPs

Purification of biogenic silver nanoparticles was carried out by a density gradient method and centrifugal forces. An optimum reaction mixture gave the maximum yield up to 79% of silver nanoparticles when reaction mixture was prepared with 1% plant extract with 0.1 molar $AgNO_3$ solution and incubated at 50 °C temperature for 48 h (Fig. 2). A similar amount of silver nanomaterial was recovered by at −8 to −20 °C thawing temperatures in the 1 L polycarbonate bottle and appeared as black layer. At low temperature reaction mixture contains particles freezing and became denser than the medium and settled down at the bottom and distinctly visible in the form of the black layer. The suspension was then centrifuged at 10,000*g* for 2 h and the particles were resuspended in ultrapure water. For the release kinetics of biogenic AgNPs, a dialysis bag was filled and sank into the buffer solution where ions were released into the medium through the dialysis

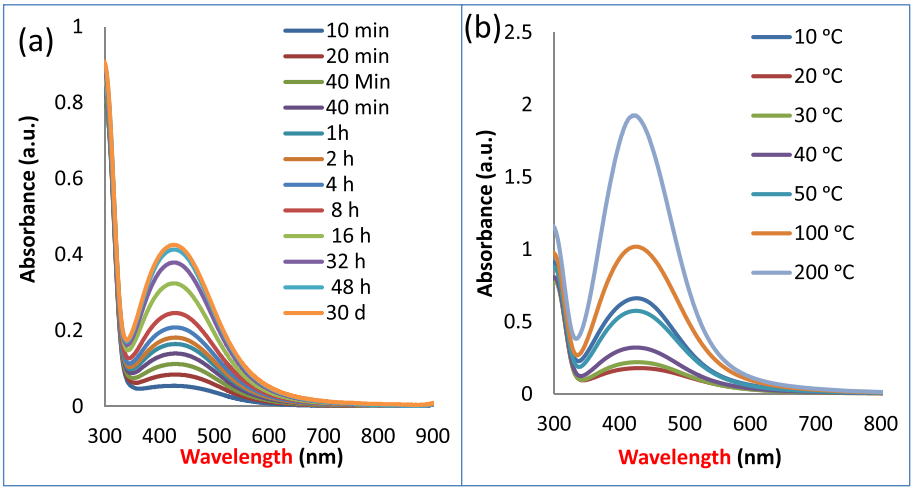

Fig. 1. UV–visible image indicate the synthesis of silver nanomaterials from plant extract (1%) and 0.1 molar silver nitrate solution peak appears at 420 nm (a) time dependent study of synthesis AgNPs, in reaction mixture, particles synthesis start just after 10 min and reaction complete after 48 h and particle stable up to 30 days at room temperature and (b) particle formation at variable temperature.

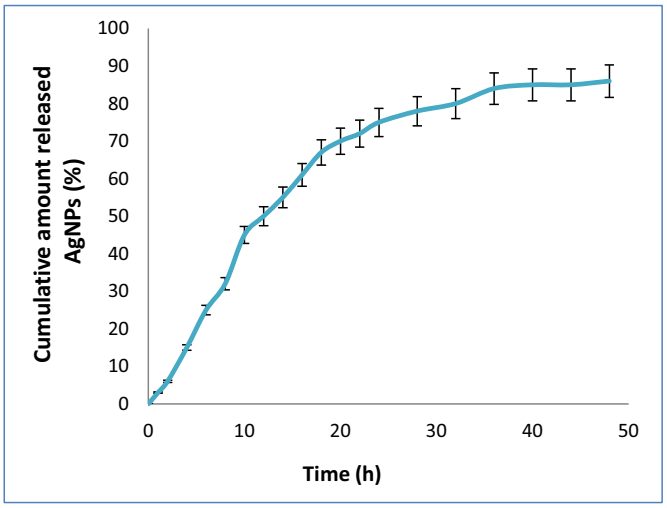

Fig. 3. Release kinetics of silver nanomaterials packed in 12 kDa cutoff dialysis bag immersed in HEPES buffer solution.

membrane. This released ion in to the medium was analyzed by atomic absorption spectrophotometer. Initially, the formation of particles in solution is lost and the low concentration of silver was released in the early stages of the experiments. A continuous release of silver ion and particles from the dialysis begs in to the medium were observed until the reaction finished at 48 h (Fig. 3). The rate of dissolution of silver followed the first order kinetics with $r^2 > 0.97$. The AgNPs release into the medium are expressed as cumulative drug released % versus time (h). At the end of the experiment maximum 86% of the AgNPs were released in the medium. The rapid release of silver ion is correlated with the particle size and its surface area. Due to the high diffusability of small-sized nanoparticles, they rapidly released than large size nanoparticles.

3.1.3. X-ray diffraction pattern

X-ray diffraction (XRD) pattern of the dried biogenic AgNPs have showed crystalline structure. The distinct XRD peaks at 2θ values of 28°, 33°, 47°, 68° and 77° (Fig. 4) can be attributed to the reflections from lattice planes 110, 111, 211, 222 and 311 sets which perfectly matched with cubic shape and the crystalline structure of silver (JCPDS file no. 04-0787). The unassigned peak at AgNPs spectrum showed the involvement of biological moieties of date root hair extract. Analyzed data shown particle size was observed 25.1 nm in mean diameter. In general, specific phase width of materials is directly proportional to the mean of material crystallite size. In our results broader peaks is the indicative of the involvement of date root hair extract in crystal nuclei growth and particle formation.

3.1.4. FTIR spectroscopy

The FTIR spectra of biogenic AgNPs derived from the date palm root extract after reaction with $AgNO_3$ and date root extract control without $AgNO_3$ are shown in Fig. 5a & b. Spectral analysis indicates marginal shift in the peak position of spectra as shown figure. This similarity in the spectra clearly depicts that date root extract is performing a dual role in the solution mixture, i.e. as a reducing and capping agent to the AgNPs. Plant root extract based AgNPs on infra-red region revealed different absorption bands between 804 and 3896 cm^{-1}. In case of AgNPs, a shift in the absorbance peak with decreased band intensity was observed at 3896 cm^{-1}. This indicates the binding of Ag with N—H and or O—H group of the date seed extract. The absorbance peak of AgNPs spectra at 1395 to 1658 cm^{-1} indicates C—H stretching vibrations of alkene whereas the peak at 1129 cm^{-1} represents the C—H in-plane bending of alkenes, alcohols, carboxylic acids, esters, and ethers. Involvement of bio-molecules in core particle matter was also investigated by Yin et al. [45]. The spectral peak at 1693 cm^{-1} in our study is predominant and indicate the involvement of amide-I bond (—C═O) of proteins as a capping agent and stabilization of AgNPs.

3.1.5. SEM, EDX, TEM and particle size distribution analysis of AgNPs

FESEM was used to analyze the surface morphology and size of biogenic AgNPs. This analysis predicts the formation and morphology of biogenically synthesized AgNPs. Using this tool, the size of biogenic AgNPs was observed ranging from 21.65 to 41.05 nm, which are mainly in uniform spherical shape (Fig. 6i). Moreover, silver metal distribution in our biogenic AgNPs was confirmed by energy dispersive X-ray (Fig. 6ii). The data obtained at a particular point, during material sample analysis which showed the involvement of silver in particle formation, whereas non-metallic residue peak also confirmed the involvement of biological moieties as a stabilizing agent which from plant

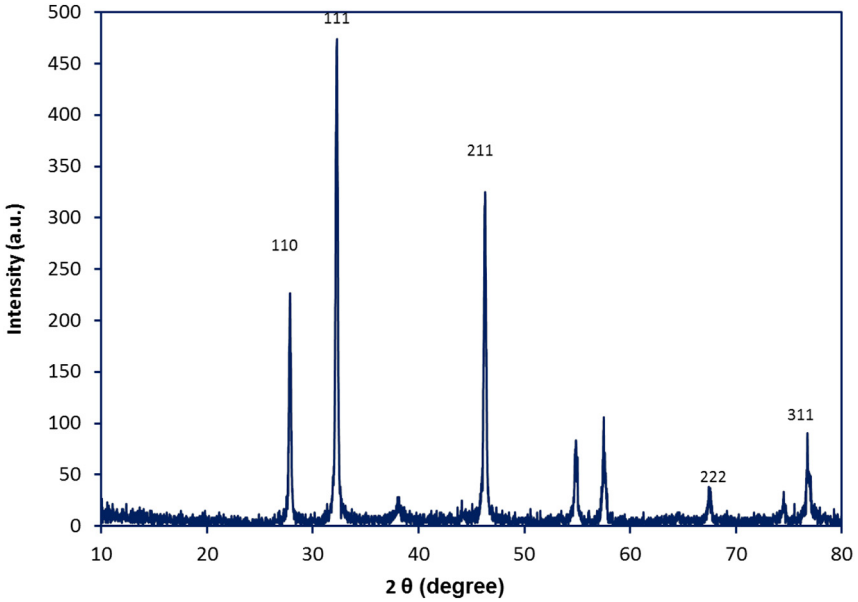

Fig. 4. The XRD graph pattern of biogenic nanomaterials synthesized from the plant extract, showing a different peak at 2Ø degree with 110°, 111°, 211°, 222° and the 311° and unknown peak of biological materials, which indicate the synthesized material is crystalline and belong to the spherical particles of silver nanomaterial.

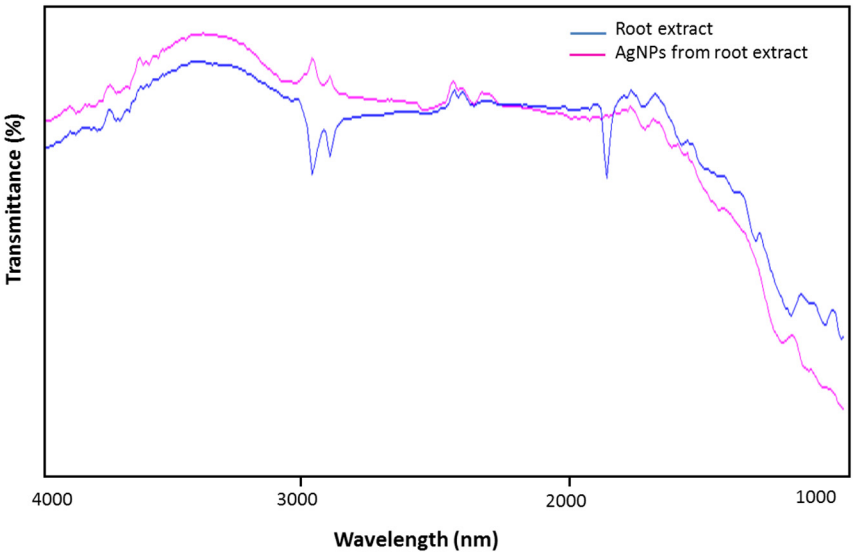

Fig. 5. FTIR image of biogenic silver nanomaterials indicated by pink line and the blue line graph indicates the biological materials extract from the plant root. The pink line graph indicates the involvement biological materials in the nanomaterial. (For interpretation of the references to color in this figure legend, the reader is referred to the web version of this article.)

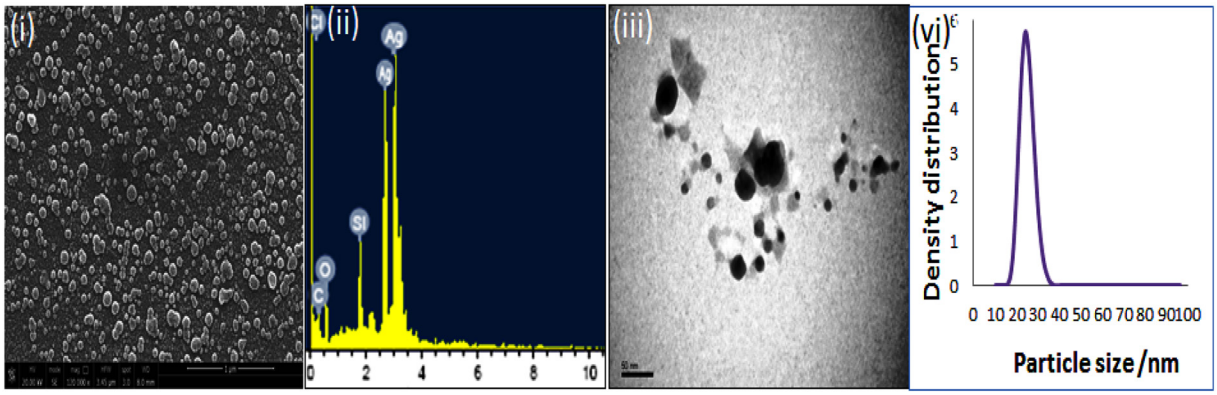

Fig. 6. Biogenic AgNPs (i) scanning electron microscopic image (ii) energy dispersive X-ray showing the involvement of silver in synthesis (iii) electron microscopic image at 50 nm scale and (iv) particle size distribution peak also indicating the particle between 15 and 41 nm in the range.

Table 2
Biogenic silver nanoparticles characteristics have obtained in this study.

Biogenic AgNPs belongings	Features
Synthesis method	Biological/bottom up approach
Stabilizing/capping agent	Aqueous extract of root hair of *Phoenix dactylifera*
Preparation period	Rapid (1 h)
Nanoparticle size	15–40 nm
UV–Vis (λ_{max})	420 nm
Mean particle diameter (X_{50})	25.01
Particle size distribution (q^3Ig)	5.74
Sauter mean diameter (SMD)	27. 28 nm
Volume mean diameter (VMD)	41.05
Specific surface area (Sv)	219. 93 m^2/cm^3
Stability	3 months
Phase	Colloidal suspension
Biocompatible	Positive
Anticancer (IC_{50})	29.6 μg/ml (MCF-7)
Antibacterial (ZI)	22 mm (*E. coli*)
Antifungal (ZI)	20 mm (*C. albicans*)

extracts (Fig. 6iii). The image scaling also confirmed the shape and size of biogenic AgNPs by transmission electron microscopy (TEM) where we observed the average AgNPs size of ~27 nm, TEM images also showed the aggregation of particles (Fig. 6iii) and distinguished spherical shaped nanoparticles (Fig. 6ii & iii). Particle size distribution in aqueous suspension was analyzed by NANOPHOX particle size analysis (Sympatec GmbH). It is a relatively new technique with Photon cross-correlation spectroscopy for the measurement of particle size, stability and distribution in opaque solution. It was applied here because it is recommended for highly diluted samples and based on special scattering geometry and the cross-correlation of the scattered light allows reliable separation of single and multiple scattered fractions. Particle size and their distributions in the reaction mixture were analyzed by Photon Cross-Correlation Spectroscopy (PCCS) NANOPHOX (Sympatec GmbH, Germany). Mean particle diameter ($\times_{50}$ = 25. 01), particle size distribution (q^3Ig = 5.74), Sauter mean diameter (SMD = 27. 28 nm), volume mean diameter (VMD = 41.05), specific surface area (Sv = 219. 93 m^2/cm^3) and particle density were found in colloidal suspension (Fig. 6iv) and summarize detail in Table 2

3.2. Antimicrobial activity

3.2.1. Zone inhibition assay

The synthesized AgNPs was tested against *E. coli* and *C. albicans* strains in order to examine the effect of green synthesized nanomaterial on microbial growth control in liquid and solid agar media. Further observed the microbial growth inhibition zone formation against *C. albicans* and *E. coli* strains, respectively (Fig. 7). The respective highest diameters of zone inhibition for both organisms were 20 and 22 mm at concentration 80 μg/well AgNPs, against *C. albicans* and *E. coli*, respectively. The zone of inhibition formation was due to the exposure of AgNPs by diffusion of silver ion in the media.

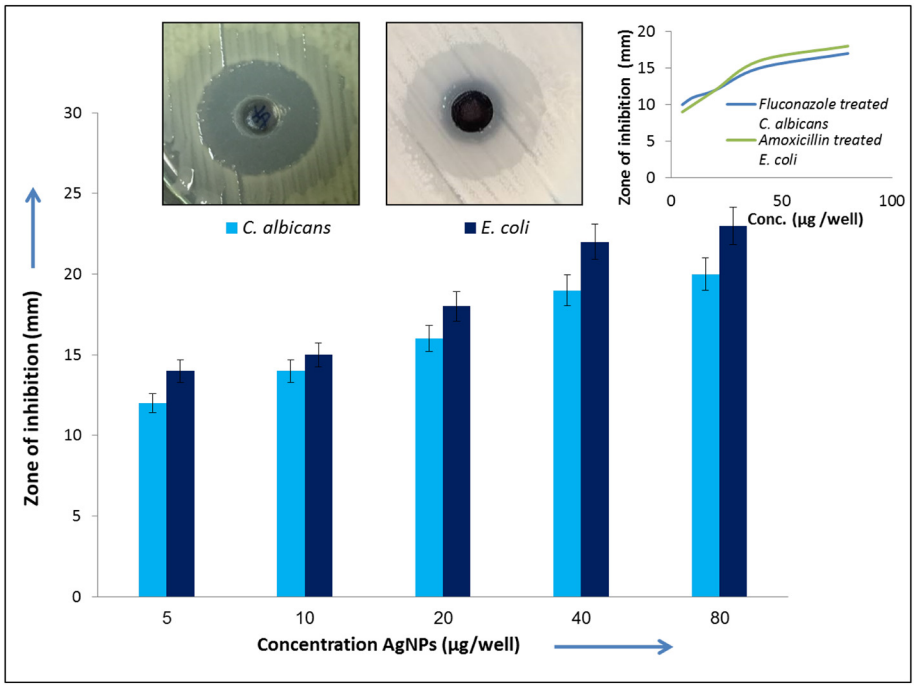

Fig. 7. Biogenic AgNPs antimicrobial activities against *C. albicans* and *E. coli* depicted in the form of zone inhibition on a solid agar plate. Maximum zone of inhibition against *C. albicans* and *E. coli* were 20 and 22 mm, respectively. The graph is showing the zone of inhibition patterns with increasing loaded concentration of AgNPs in well.

3.2.2. Growth kinetic, potency and interfacial interaction study

To get a further understanding of antimicrobial action and microorganism interaction with nanomaterial, microorganism treated with nanomaterial at various concentrations (0, 5, 10, 20 and 40 µg/ml AgNPs) and measures the growth kinetic with microbial growth. The influence of AgNPs concentration on the cell viability was judged by comparing scanning electron microscopy images of control and AgNPs treated cultures. Significant growth inhibition was observed when *E. coli* and *C. albicans* strains were treated with 20 µg/ml of AgNPs and incubates for 2 and 48 h (Fig. 8a & b). We also checked the potency of AgNPs against both organisms and found 100% microbicidal at 40 µg/ml. Untreated culture (control) and treated culture was analyzed by SEM. The results depicted in figure (Fig. 9a vs. b and c vs. d) Indicate the clumping/aggregation of bacterial and fungal cells compared with control. This is a clear indication of viable fungi and bacteria cells in SEM images (Fig. 9a and c). However, images of these organisms treated with AgNPs revealed the non-viability of both bacterial and fungal cells through rupturing of membranes or blebs in case of fungal strains and the complete disintegration of cell walls in case of *E. coli*. The presence of elemental silver in the membrane structure of both pathogenic bacteria and fungi was confirmed by EDAX analysis (Fig. 9b and d). These observations confirmed the incorporation of AgNPs into the membranes of microbes and generation of free radicals with membrane lipid which enhances autolysis of cells. Hence, the permeability of membrane changes which may cause the membrane degradation of *E. coli*. Furthermore, nanomaterials treated culture growth activity checked by culture spread plate method on nutrient agar plate and find the increasing dose AgNPs enhances the bactericidal activity and incubated plate with decreasing number of colony (Fig. 10).

3.3. Hemolysis assay

The most important facet of any drug is that it should be biocompatible in nature i.e. it should be non-toxic toward healthy cells. In order to check the biocompatible nature of our synthesized AgNPs, we performed RBC lysis test. The pre-incubation of our synthesized NPs with RBCs showed very little toxicity and caused limited lysis of cells. As shown in Fig. 11a, 18.6% ($P \leq 0.001$) hemolysis of cells was observed at high dose 256 µg/ml of AgNPs which is very less in compare to the Triton X100, thus suggesting its biocompatibility. However, with increasing concentration, the cell viability was found to be proportionally decreased.

3.4. Cytotoxicity assays

Peripheral blood mononuclear cells (PBMCs) were employed to confirm the biocompatibility of materials. Biogenic AgNPs did not show any cytotoxic effects on PBMCs even at 5 times higher dose of the MIC concentration (~100 µg/ml). However, a further increase in the dose causes cell death shown in Fig. 11b. The MTT results established a concentration-dependent cytotoxicity of AgNPs, after their exposure to MCF-7 cells, Fig. 11c. The cell viability was found to be decreased with increasing concentration of AgNPs in time-dependent manner. The reduction of MTT decreases with an increase in the concentration of AgNPs, IC_{50} was found to be around the 29.6 µg/ml (Fig. 12).

3.4.1. Dual AO/EtBr staining to detect apoptosis

The apoptotic potential of AgNPs was further established by dual AO/EtBr staining. The control group demonstrated green fluorescence only. However, following the treatment of AgNPs early-stage apoptotic cells were marked by a crescent-shaped or granular yellow-green acridine orange nuclear staining. Late-stage apoptotic cells were marked with focused and lopsidedly localized orange nuclear ethidium bromide staining. On the other hand, necrotic cells increased in volume and showed uneven, orange-red fluorescence at their periphery (Fig. 13).

3.4.2. Cell cycle analysis

After establishing the cytotoxic potential of AgNPs on MCF-7 cells, we evaluated their potential to modulate the cell cycle progression. Upon the treatment of MCF-7 cells with 15 µg/ml AgNPs for 24 h, around 48.90% of cells were observed in G1 phase and 18.01% in G2/M phases of cell cycle. While at a higher dose of 30 µg/ml AgNPs, 41.60% ($P \geq 0.01$) and 16.58% ($P \geq 0.001$) cells were found to be in G1 and G2/M phases as compared to control untreated cells that are found to be around 56.76% and 21.7% in G1 and G2/M phases of cell cycle respectively (Fig. 14). The increase in cell population in the said phases was at the expense of S-phase cell population. The data suggest that cell growth inhibition by AgNPs may be accompanied by induction of cell

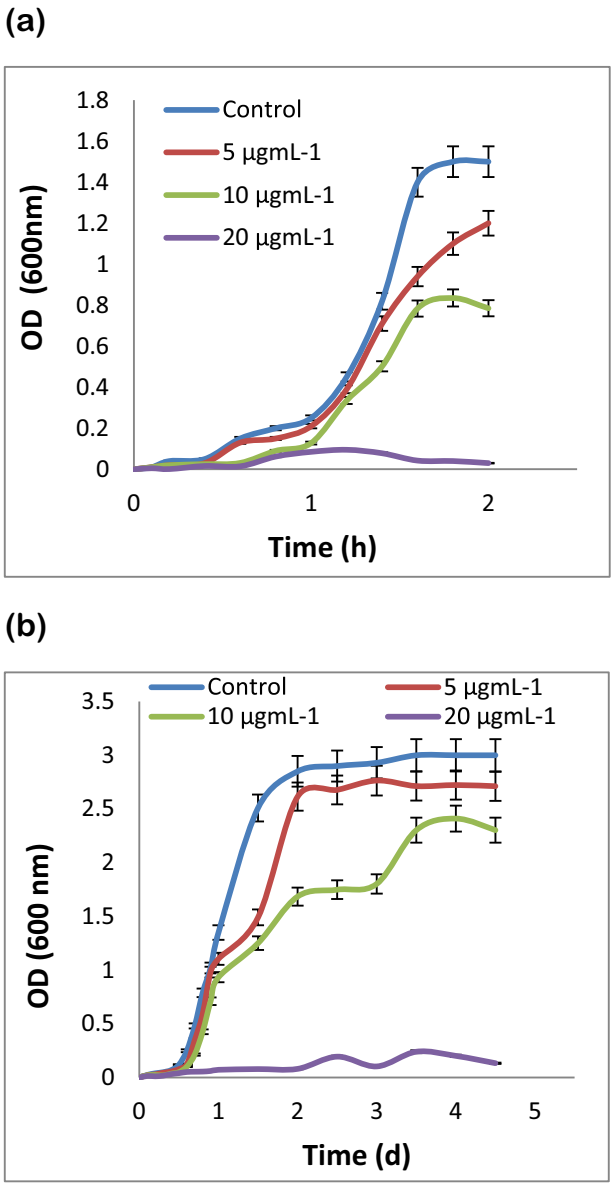

Fig. 8. Antimicrobial effect of biogenic AgNPs in broth media (a) *E. coli* growth pattern in the absence (control) and presence of different dose of AgNPs for 2 h incubation at 35 °C (b) *C. albicans* growth pattern in the absence (control) and the presence of different doses of AgNPs amended in growing media with 4 days incubation at 35 °C.

cycle arrest with a reduced number of proliferating cells in S-phase.

4. Discussion

4.1. UV–vis spectra analysis of green synthesized nanoparticles

Biogenic synthesis of AgNPs was carried out by the reduction of Ag^+ to Ag^0 in $AgNO_3$ solution through the aqueous plant root extract at variable time and temperature. After 48 h, development of light to dark brown color indicated the reduction of silver ion in elemental form which was confirmed by maximum absorption peak between 418 and 420 nm (Fig. 1a). The color appeared in the solution was due to the formation of AgNPs which exhibited surface plasmon resonance (SPR) [46]. Thus, change in color and λ_{max} with prominent peak at 420 nm correspond to AgNPs formation. Optical absorption spectrum of AgNPs indicated by SPR revealed a band pattern (Fig. 1a) that could be linked to size, shape, and particle aggregation as well as their distribution. Moreover, the shift in band patterns indicates that the electron movement of silver nanomaterials in the reaction mixture was very high and could be observed by the closeness between the conduction band and valence band. The collective oscillation of electron movement on AgNPs surface may give rise to a band of SPR absorption in the visible region. Our UV–vis SPR results are in agreements with recent studies on organic coated green synthesized silver nanomaterials [47]. We have also investigated the effect of temperature and time on the AgNPs synthesis (Fig. 1a & b) productivity and production efficiency. For this purpose, we optimized the concentration of $AgNO_3$, volume of date root extract and time at 48 h of incubation at optimum 50 °C temperature. The UV–Vis spectra were recorded from date root hair extract at different reaction times (Fig. 1a & b). We found that the formation of AgNPs started after 10 min of incubation and reaction was successfully completed within 48 h. The spectrum indicates the presence of a strong SPR curve between 410 and 430 nm with peak centered at 420 nm (Fig. 1a). This peak is a characteristic of colloidal brown, silver [48]. Our results are in accordance with earlier reports by Ahmad et al. [49] and Sharma et al. [47], who observed that incubation of green materials with $AgNO_3$ solution result in the synthesis of AgNPs with λ_{max} of 436 nm. Moreover, UV–vis spectra indicate an increase in the absorbance intensity of the reaction mixture with time (Fig. 1b) and after 48 h no further increase in SPR was observed after 30 days similar SPR was observed of the sample. These observations indicate that an increased number of AgNPs was synthesized in the mixture with time and after 48 h no further increase in formation of nanomaterials occurred, which indicates the completion of reaction in the solution. To study the effect of temperature, we synthesized AgNPs at various temperature; 10, 20, 30, 40, 50, 100 and 200 °C. Our UV–vis spectra results indicated that the synthesis of AgNPs using plant root hair extract was increased at elevated temperature of 200 °C (Fig. 1b). Our findings are in accordance with Khan et al. [50] who also observed the temperature dependence on the formation of AgNPs using *P. glutinosa* extract. Similar to our study, they also obtained higher production of AgNPs at higher temperature. However, when the temperature was increased to above 40 °C there was a shift in SPR peak toward longer wavelength which indicates an increase in particle size [50]. This was also confirmed by the results obtained from the NANOPHOX particle size analyzer which observed the synthesis of AgNPs at varying temperature and increase in size with temperature. From this observation, it was confirmed that AgNPs synthesized from date root hair extract was temperature dependent and optimum temperature of 50 to 100 °C for the formation of ~27 nm particles. Likewise, at 55 °C temperature and very short time period (10 min) silver nanoparticles were synthesized from the fruit extract of date palm by Farhadi et al. [19].

4.2. Purification and release kinetics

Purification of biogenic nanomaterials is an important step and most of the studies lack this part due to insufficient knowledge. Biologically synthesized nanomaterials contained unused biological moieties and silver nitrate solution in colloidal suspension. In this study silver nanomaterials purified by density gradient, centrifugal force and deep freeze thawing methods and approx 79% yield was observed from the 1% plant extract after 48 h incubation at 50 °C. The AgNPs yield decreases sharply when more plant extract was added in the reaction mixture (Fig. 2). Similarly, some studies have also reported the purification of AgNPs by variable deep freeze temperature and density gradient methods [38,51]. Hahn et al. [52] reported the release kinetics of dissolution of the nanoparticle as anisotropic and described by pseudo-first-order exponential equation.

The dissolve silver ion is responsible for the decontamination of the microbial agent in an aqueous system, but it is necessary to understand the release kinetics of ions from the particles in the surrounding medium. In most of the cases, small particles release ions and easily disperse and precipitate due to the interaction with other particles.

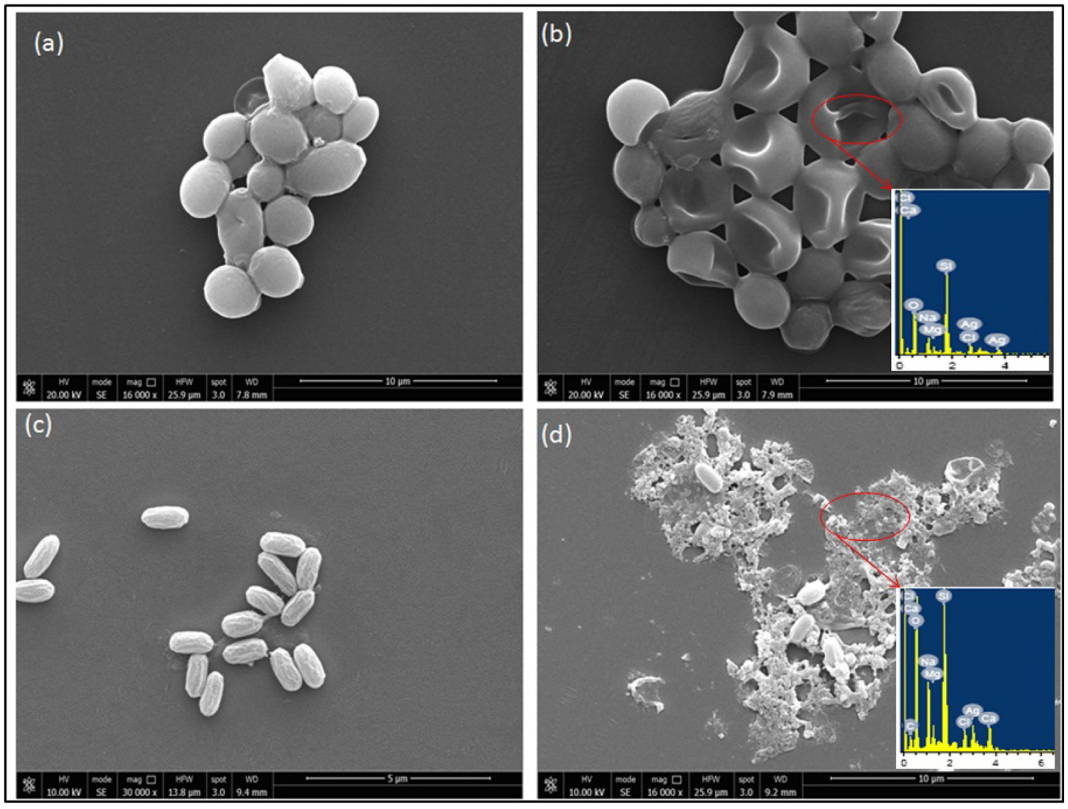

Fig. 9. Antimicrobial activities of biogenic AgNPs confirmed by scanning electron microscopy (SEM) and microbicidal role confirmed by energy dispersive X-ray analysis, (a) untreated AgNPs *C. albicans* served as a control (b) 20 μg/ml AgNPs treated in liquid media *C. albicans* after overnight growth clearly showing blebs in cell and prevent the growth multiplication (c) untreated *E. coli* served as control and (d) 20 μg/ml AgNPs amended in nutrient broth after 4 h of incubation, clearly shown the distorted cell.

When the released Ag ion and its concentration reached at the certain limit and solution gets equilibrium through the cooperative oxidation by the involvement of protons and dissolved available oxygen. However, released ions can rejoin and form aggregates of existing nanoparticles. In this study within 48 h, the concentrations of Ag ions increased exponentially up to 86%. An earlier study on the release kinetics of Ag ions reported that the release reaction follows first-order kinetics [53].

4.3. FTIR spectroscopy

The FTIR spectra of AgNPs derived from plant extract after reaction with $AgNO_3$ (Fig. 4a) and date root extract (Fig. 4b) control without $AgNO_3$ are shown in Fig. 4. Spectral analysis indicates a marginal shift in the peak position of spectra a, and b (Fig. 4). These findings are in line with other studies where the spectral peak was observed between 3199 and 3314 cm^{-1} and correspond to N—H, and O—H stretching vibrations of 1°, and 2° amines, amides, alcohol, and H–bonded phenols. This similarity in the spectra clearly indicates that plant extract is performing a dual role in the solution mixture, i.e. as a reducing and capping agent to the AgNPs. Our findings of the FTIR spectra analyses are in accordance with those of Khan et al. [50] and Basu et al. [54] who reported similar trends in the FTIR spectra of the synthesized AgNPs through green material extract. Date palm root hair extracts

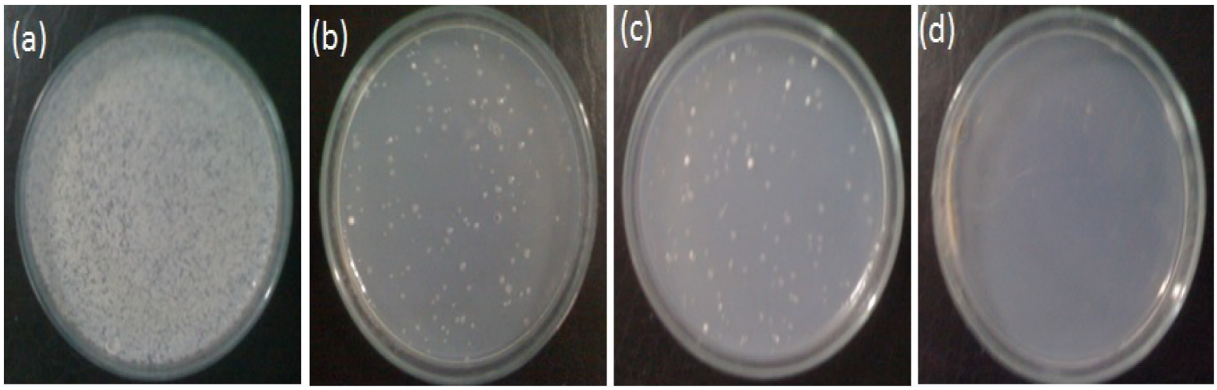

Fig. 10. Antimicrobial image of plates, *E. coli* cultured on silver nanomaterials containing nutrient agar plate (a) without silver nanoparticles (control) which showed a lawn of *E. coli* on the plate surface (b) plate containing 10 μg/ml AgNPs in the media showing numbers of discrete colonies of bacteria on plates and concentration reveal its minimum inhibitory concentration (MIC) and (c) plate amended with 20 μg/ml AgNPs number of colonies lesser than b plate and (d) plate with 40 μg/ml AgNPs, no growth of bacteria found after overnight incubation which represented a minimum bactericidal concentration (MBC).

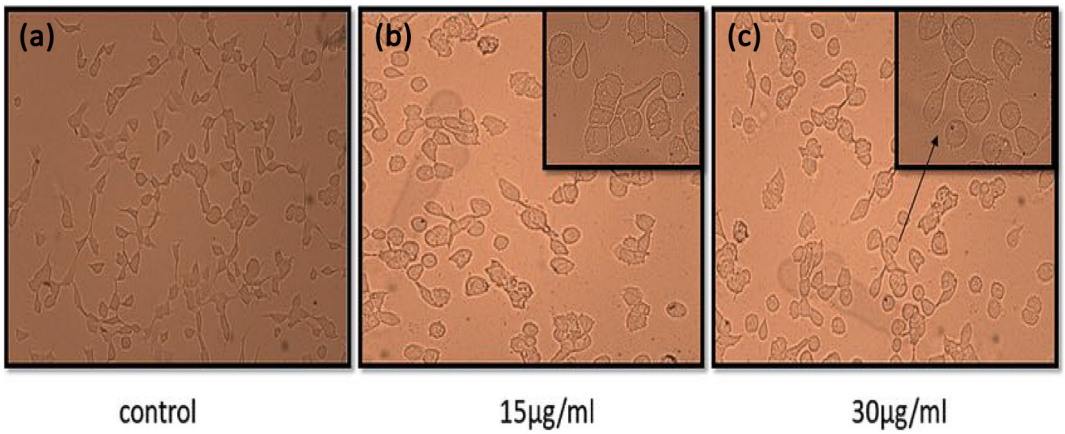

Fig. 11. Biogenic silver nanomaterials anticancer activity against breast cancer cell line MFC-7 (a) untreated cells (b) cell morphology at 15 µg/ml treatment (c) cell morphology at 30 µg/ml treatment showing a little bit distorted shape.

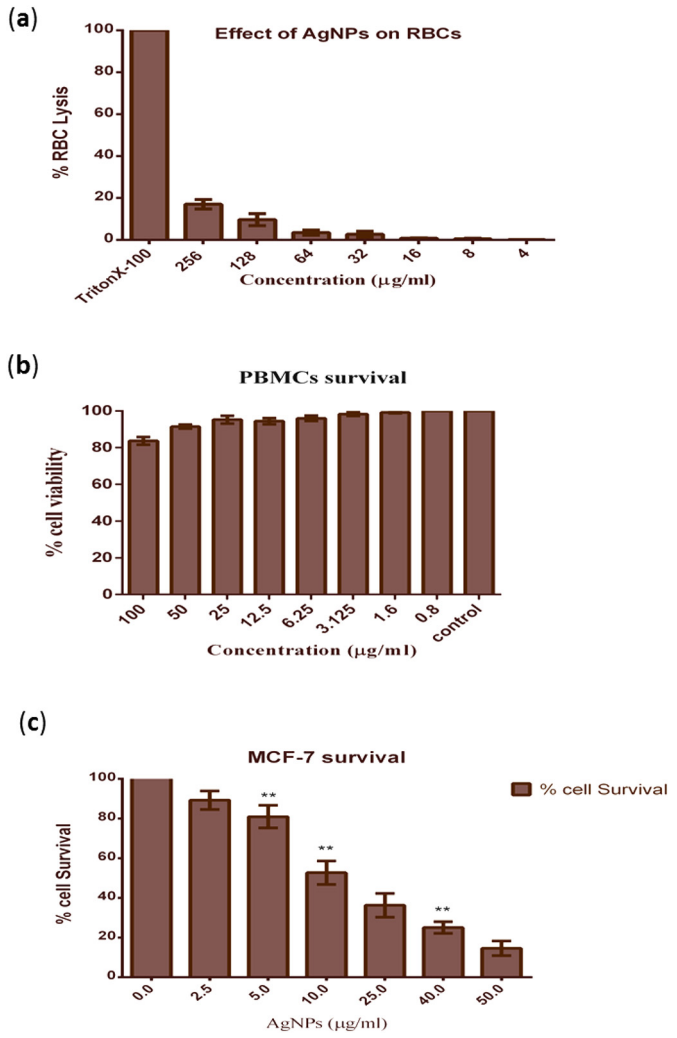

Fig. 12. Effect of varying concentration of AgNPs on RBCs leakage (a). Effect of AgNPs on the viability of cells, PBMCs (normal cells) after treatment in a dose dependent manner after 24 h (b). MCF-7 cells viability was determined by using MTT assay (c), data represented here mean ± standard deviation of three identical experimental data.

based AgNPs on infra-red region revealed different absorption bands at 3896, 3828, 3453, 2998, 2803,2658, 2486, 2211, 1744, 1481, 1392, 1289, 1188, 1023, 904, 804 cm^{-1} (Fig. 4). In case of AgNPs, a shift in the absorbance peak with variable band intensity was observed at different points (Fig. 4). This indicates the binding and capping of Ag with biological functional groups like N—H and O—H group from the plant extract. These findings are in line with other studies where the spectral peak was observed between 2998 and 3453 cm^{-1} and corresponding to N—H, and O—H stretching vibrations of 1° and 2° amines, amides, alcohol, and H–bonded phenols [55]. The absorbance peak of AgNPs spectra at 1395 to 1658 cm^{-1} indicates C—H stretching vibrations of alkene [55] whereas the peak at 1129 cm^{-1} represents the C—H in-plane bending of alkenes, alcohols, carboxylic acids, esters, and ethers [56]. Involvement of bio-molecules in core particle matter was also investigated by Ankamwar et al. [57]. In their study, spectra revealed a band at 2211 cm^{-1} and were assigned to the N—H stretching band in the free amino groups of silver nanoparticles. The spectral peak at 1593 cm^{-1} in our study is predominant and indicates the involvement of the amide bond (—C═O) of proteins as a capping agent and stabilization of AgNPs. Moreover, the peak present at 804 cm^{-1} with the AgNPs spectrum in addition to other peaks in date seed extract spectrum indicates the banding of AgNPs with oxygen from —OH groups in date seed compounds. This finding was justified by the reduction of Ag^{+} and stabilizing the nanomaterial by the biological functional group earlier reported by Pacioni et al. [58].

4.4. X-ray diffraction pattern

XRD pattern analysis of the biogenic AgNPs confirmed the crystalline nature of synthesized materials. A number of peaks appeared on 2 theta angle during sample analysis at the variable wavelength. These reflections have a good correlation with Bragg's reflections. Moreover, the peaks present at 29.60° near 31.9° show the presence of Ag_2O [59]. The unassigned peak at AgNPs spectrum showed the involvement of biological moieties of date root extract in material synthesis. Analyzed data file number PDF#04-0787 and crystallite size was observed at 21.5 nm in particle formation. In general, specific phase width of materials is directly proportional to the mean of material crystallite size. The broader peaks are indicative of the smaller crystallite size [60,61]. In our results broader peaks indicate the involvement of date plant root hair extract in crystal nuclei growth and particle formation. This result is also in good agreement with the XRD patterns were observed by Becheri et al. [62].

4.5. Field emission scanning electron microscopy (FESEM) and transmission electron microscopy (TEM) analysis

FESEM was used to analyze the surface morphology of biogenic AgNPs. Using this technique, we observed the size of biogenic AgNPs

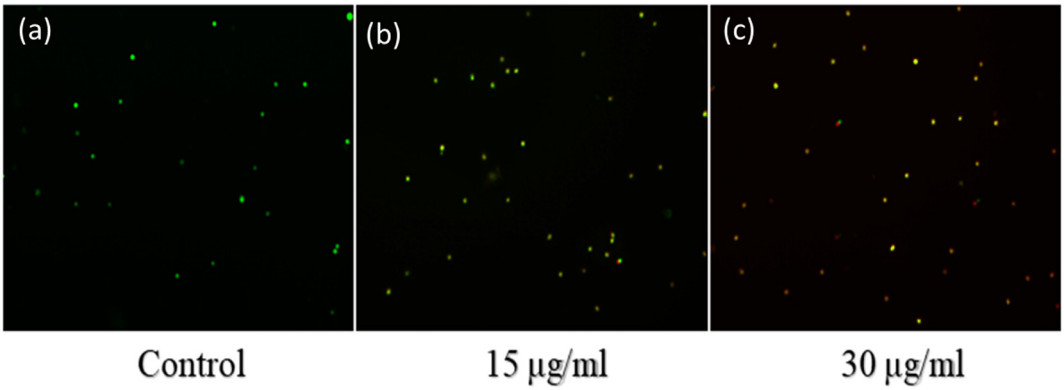

Fig. 13. AgNPs induced apoptosis in MCF-7 cells as revealed by AO-EtBr assay: Normal cells show circular nucleus uniformly distributed in the center of the cell. Untreated experimental group. (a); cells treated with 15 µg/ml (b) and 30 µg/ml (c) showed yellow-green fluorescence corresponding to acridine orange (AO) staining and concentrated orange nuclear ethidium bromide staining. (For interpretation of the references to color in this figure legend, the reader is referred to the web version of this article.)

ranging from 15 to 41 nm, mainly in uniform spherical shape (Fig. 6a). Moreover, silver metal distribution in our biogenic AgNPs was confirmed by energy dispersive X-ray. The data obtained at a particular point of gold-coated sample showed the silver involvement in particle formation, whereas non-metallic residue confirmed the involvement of biological moieties from date plant extract (Fig. 6b). We also confirmed the shape and size of biogenic AgNPs by TEM, where we observed the average AgNPs size of ~27 nm. TEM images also showed the aggregation of particles (Fig. 6a) and distinguished spherical shaped nanoparticles (Fig. 6a, b). The size of the synthesized AgNPs by us is in line with Bar et al. who also reported 50 nm size of AgNPs from the seed extract of *Jatropha curcas* [13].

4.6. Antimicrobial activity

The synthesized AgNPs were tested against bacterial and fungal strains in order to examine the effect of green synthesized nanomaterial on microbial growth inhibition. Applied concentration of nanomaterials produced dark color on the sides of the wells (Fig. 7). This could probably be due to the higher concentration of the applied AgNPs which may disappear after optimized dilutions. The respective diameters of inhibition zones for both organisms were 20 and 22 mm. The inhibition zone observed in the case of *E. coli* was much larger than reported by Kahrilas et al. [63]. The difference in growth inhibition zone in our study and reported literature could be explained by variation in concentrations of the exposed AgNPs or due to higher diffusion of nanomaterials in the nutrient media. For further understanding of this interaction, a growth kinetic study was performed using various concentrations (0, 5, 10, 20, 40, 80 and 100 µg/ml) of AgNPs suspension on the microbial growth. The influence of AgNP concentration on the cell viability was judged by comparing SEM images of control and AgNPs treated cultures. Significant growth inhibition of both bacteria

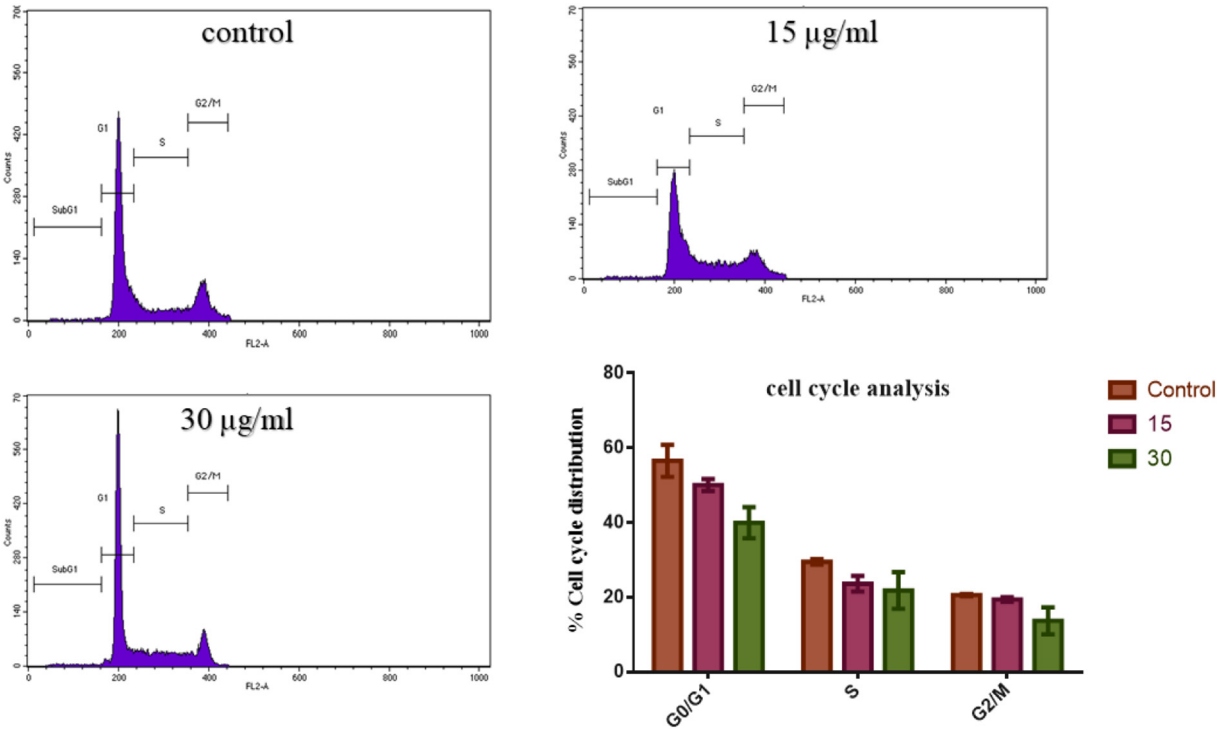

Fig. 14. Effect of AgNPs on cell cycle progression of MCF-7 cells. Cells were treated for 24 h and processed and analyzed by flow cytometry. The percentage of cell cycle distribution data of cells are shown as mean ± SE of triplicate samples for three independent experiments (*P ≤ 0.001; #P ≤ 0.05).

and fungi strains was observed when cultures were treated for 8 h with 20 μg/ml of AgNPs. 100% potency of 40 μg/ml of AgNPs was observed against both organisms after overnight growth (Fig. 8). Our results are in accordance with Sun et al. [59] who have reported the inhibition in the growth of *E. coli* by AgNPs synthesized from tea leaf extract. They further explained that AgNPs could attach to the bacterial cell wall or releases free radicals that can inhibit the growth of bacteria. AgNPs in our study was shown to damage the cell membranes of *E. coli* and *C. albicans*; the formation of pits or grooves in the membranes of later organisms and destruction of whole cells in case of former microbe (Fig. 9b & d). The presence of elemental silver in the membrane structure of both pathogenic bacteria and fungi was confirmed by EDAX analysis (Fig. 9a & b). These observations confirmed the incorporation of AgNPs into the membranes of microbes. Our observations are in accordance with those of Amro et al. [64] where they explained that the metal depletion from microbial cells may cause the formation of pits or grooves in the outer membrane. These pits are formed by the regular release of lipopolysaccharides molecules and membrane proteins. Hence, the permeability of membrane changes which may cause the membrane degradation of *E. coli*. The antifungal activity of our synthesized AgNPs is also significantly collinear with earlier reports [65,66].

4.7. Biocompatibility and cytotoxicity assay

4.7.1. Hemolysis assay

Nanotechnology based drugs have a high potential to the treatment and diagnosis of cancer and infection related diseases [67]. Most of the therapeutic nanoparticles are administrated through oral and intravenous system after that they directly interact with blood component which generates a number of responses. In this context, we have also analyzed the exposure of AgNPs on red blood cells. The pre-incubation of our synthesized NPs with RBCs showed very little toxicity and causes limited lysis of cells. Synthesized nanomaterial causes hemolysis of cells at a very high concentration (256 μg/ml), thus suggesting its biocompatibility (Fig. 11). In previous studies, amorphous nanomaterials like silica, tricalcium phosphate and hydroxyapatite nanoparticles have been employed in RBC lysis and proved inclined hemolysis rate with increasing concentration > 5% at 1000 μg/ml [68,69]. While in case of silver nanoparticles a very low hemolytic activity has been reported as compared to $AgNO_3$ [70]. Several factors like a silver ion release, increased surface and smaller size of nanoparticles could be the reason behind the low rate of RBC lysis [71,72].

4.7.2. Cytotoxicity assay

In this study, MTT assay of biogenic AgNPs showed that the significant cytotoxicity against the MCF-7 cell line. The cell viability was found to be decreased with an increase in the concentration of AgNPs in time-dependent manner. The reduction of MTT decreases with an increase in the concentration of AgNPs, IC50 was found to be around 29.6 μg/ml. These results are well-coordinated with previous study where AgNPs were synthesized from the *Pleurotus ostreatus* extract. They also observed a dose-dependent inhibition of cell proliferation and achieved up to 5% inhibition of cell growth at 80 μg/ml AgNPs concentration [47]. Moreover, our results also agree with an earlier study on green *Cannonball leaves* synthesized AgNPs cytotoxicity against MCF7 cells [73]. Similarly, *M. pulegium* extract mediated biogenic silver nanoparticles was also reported in previous studies as an anticancer agent, when employed against HeLa and MCF-7 cancer cells [74].

Apoptosis is a biochemical event inside the cell which leads to the programmed cell death. It is a control process which elicits in certain stress condition to regulate the turnover of organelles and proteins within cells. Sometimes it is able to degrade cytoplasmic content like unfolded proteins and cell organelles. In this study, AgNPs induce apoptosis in MCF-7 cells was determined by the dual staining by acridine orange and ethidium bromide. The control group demonstrated green fluorescence only while AgNPs treated in early-stage apoptotic cells becomes yellow-green and late-stage becomes orange due to necrosis which depends on treating concentration. In a recent study, biogenic silver nanoparticles synthesized from the leaf extract of *Adenium obesum* showed similar dose dependent apoptosis [75]. Some studies also reported cell death mechanism when treated with nanomaterials [76,77]. Furthermore, we also analyzed the cell cycle of AgNPs treated MCF-7 cell and modulated cell progression. In this study, AgNPs treated cell cycle was found to be arrested in S-phase and significantly reduces the cell proliferation. Likewise, cell progression was found to be arrested in sub-G1 and S-phase and unable to enter M phase when MCF-7 cells were treated with metallic nanoparticles [78].

5. Conclusion

In the present piece of work, we have successfully synthesized silver nanomaterial from the root hair extract of *Phoenix dactylifera* and demonstrated their application against medically important pathogens and cancer cell line. In nanoparticles preparation biological plant root extract act as a silver ion reducing, capping and establishing agent. In this study, adopted a nanoparticles synthesis method was very easy, rapid and environmentally friendly without any involvement of energy consuming steps. Furthermore, synthesized materials were applied for biological activities like anticancer against breast cancer cell line (MCF-7) and antimicrobial against *E. coli* and *C. albicans*. Overall, we conclude these biogenic nanomaterials are biocompatible and an effective therapeutic agent against bacterial, fungal infections and cancer treatment. This biogenic AgNPs could also serve as a boon for the treatment of cancer especially breast cancer.

Acknowledgments

This research work is based on the green, sustainable technology and development of biogenic nanomaterials, supported by the Center of Excellence in Environmental Studies and Ministry of Higher Education, King Abdulaziz University, Jeddah, Kingdom of Saudi Arabia.

References

[1] A. Haider, I.K. Kang, Preparation of silver nanoparticles and their industrial and biomedical applications: a comprehensive review, Adv. Mater. Sci. Eng. 16 (2015) 165257.
[2] S. Mishra, B.R. Singh, A.H. Naqvi, H.B. Singh, Potential of biosynthesized silver nanoparticles using *Stenotrophomonas* sp. BHU-S7 (MTCC 5978) for management of soil-borne and foliar phytopathogens, Sci. Report. 7 (2017) 45154.
[3] H. Bagheri, S. Banihashemi, Sol-gel-based silver nanoparticles-doped silica–polydiphenylamine nanocomposite for micro-solid-phase extraction, Anal. Chim. Acta 886 (2015) 56–65.
[4] S. Ueno, K. Nakashima, Y. Sakamoto, S. Wada, Synthesis of silver-strontium titanate hybrid nanoparticles by sol-gel-hydrothermal method, Nanomater. (Basel) 5 (2015) 386–397.
[5] K. Ali, B. Ahmed, S. Dwivedi, Q. Saquib, A.A. Al-Khedhairy, J. Musarrat, Microwave accelerated green synthesis of stable silver nanoparticles with *Eucalyptus globulus* leaf extract and their antibacterial and antibiofilm activity on clinical isolates, PLoS One 10 (2015) e0131178.
[6] S.B. Maddinedi, B.K. Mandal, S.K. Maddili, Biofabrication of size controllable silver nanoparticles - a green approach, J. Photochem. Photobiol. B 167 (2017) 236–241.
[7] P. Azmath, S. Baker, D. Rakshith, S. Satish, Corrigendum to "Mycosynthesis of silver nanoparticles bearing antibacterial activity", Saudi Pharm. J. 24 (2016) 140–146.
[8] N. Jayaprakash, J.J. Vijaya, K. Kaviyarasu, K. Kombaiah, L.J. Kennedy, R.J. Ramalingam, M.A. Munusamy, H.A. Al-Lohedan, Green synthesis of Ag nanoparticles using Tamarind fruit extract for the antibacterial studies, J. Photochem. Photobiol. B 169 (2017) 178–185.
[9] C. Krishnaraj, E.G. Jagan, S. Rajasekar, P. Selvakumar, P.T. Kalaichelvan, N. Mohan, Synthesis of silver nanoparticles using *Acalypha indica* leaf extracts and its antimicrobial activity against water borne pathogens, Colloids Surf. B: Biointerfaces 76 (2010) 50–56.
[10] A. Saxena, R.M. Tripathi, F. Zafar, P. Singh, Green synthesis of silver nanoparticles using an aqueous solution of *Ficus benghalensis* leaf extract and characterization of their antimicrobial activity, Mater. Lett. 67 (2012) 91–94.
[11] A.M. Awwad, N.M. Salem, Green synthesis of silver nanoparticles by mulberry leaves extract, Nanosci. Nanotechnol. 2 (2012) 125–128.
[12] V.K. Vidhu, A. Aromal, D. Philip, Green synthesis of silver nanoparticles using *Macrotyloma uniflorum*, Spectrochim. Acta A 83 (2011) 392–397.

[13] H. Bar, D. Bhui, G.P. Sahoo, P. Sarkar, S. Pyne, A. Misra, Green synthesis of silver nanoparticles using seed extract of *Jatropha curcas*, Colloids Surf. A Physicochem. Eng. Asp. 348 (2009) 212–216.

[14] C. Luna, V.H.G. Chávez, E.D. Barriga-Castro, N.O. Núñez, R. Mendoza-Reséndez, Biosynthesis of silver fine particles and particles decorated with nanoparticles using the extract of *Illicium verum* (star anise) seeds, Spectrochim. Acta A 141 (2015) 43–50.

[15] B. Sadeghi, A. Rostami, S.S. Momeni, Facile green synthesis of silver nanoparticles using seed aqueous extract of *Pistacia atlantica* and its antibacterial activity, Spectrochim. Acta A Mol. Biomol. Spectrosc. 134 (2015) 326–332.

[16] Y.S. Rao, V.S. Kotakadi, T.N. Prasad, A.V. Reddy, D.V. Saigopal, Green synthesis and spectral characterization of silver nanoparticles from Lakshmi tulasi (*Ocimum sanctum*) leaf extract, Spectrochim. Acta A Mol. Biomol. Spectrosc. 103 (2013) 156–159.

[17] E. Geethalakshmi, D.V. Sarada, Synthesis of plant-mediated silver nanoparticles using *Trianthema decandra* extract and evaluation of their anti microbial activities, Int. J. Eng. Sci. Technol. 2 (2010) 970–975.

[18] S. Al-daihan, R.S. Bhat, Antibacterial activities of extracts of leaf, fruit, seed and bark of *Phoenix dactylifera*, Afr. J. Biotechnol. 11 (2014) 42.

[19] S. Farhadi, B. Ajerloo, A. Mohammadi, Green biosynthesis of spherical silver nanoparticles by using date palm (*Phoenix dactylifera*) fruit extract and study of their antibacterial and catalytic activities, Acta Chim. Slov. 64 (2017) 129–143.

[20] M. Khatami, S. Pourseyedi, *Phoenix dactylifera* (date palm) pit aqueous extract mediated novel route for synthesis, high stable silver nanoparticles with high antifungal and antibacterial activity, IET Nanobiotechnol. 9 (2015) 184–190.

[21] M.I. Rashid, L.H. Mujawar, Z.A. Rehan, H. Qari, J. Zeb, T. Almeelbi, I.M.I. Ismail, One-step synthesis of silver nanoparticles using *Phoenix dactylifera* leaves extract and their enhanced bactericidal activity, J. Mol. Liq. 223 (2016) 1114–1122.

[22] A.K. Mittal, D. Tripathy, A. Choudhary, P.A. Aili, A. Chatterjee, et al., Bio-synthesis of silver nanoparticles using *Potentilla fulgens* Wall. ex Hook. and its therapeutic evaluation as anticancer and antimicrobial agent, Mater Sci Eng C Mater Biol Appl 53 (2015) 120–127.

[23] J. Venkatesan, S.K. Kim, M.S. Shim, Antimicrobial, antioxidant, and anticancer activities of biosynthesized silver nanoparticles using marine algae *Ecklonia cava*, Nanomaterials 6 (2016) 235, http://dx.doi.org/10.3390/nano6120235.

[24] A.P. Kanjikar, A.L. Hugar, R.L. Londonkar, Characterization of phyto-nanoparticles from *Ficus krishnae* for their antibacterial and anticancer activities, Drug Dev. Ind. Pharm. 44 (2018) 377–384, http://dx.doi.org/10.1080/03639045.2017.1386205.

[25] A.F. da Cruz Paula, Characterization of Different Breast Cancer Stem Cell Phenotypes in Proliferative, Pre-malignant and Neoplastic Lesions of the Breast: Associations With Breast Cancer Behavior and Progression, (2016).

[26] D. Wang, J. Markus, Y.J. Kim, C. Wang, Z.E. Jiménez Pérez, S. Ahn, V.C. Aceituno, R. Mathiyalagan, D.C. Yang, Coalescence of functional gold and monodisperse silver nanoparticles mediated by black *Panax ginseng* Meyer root extract, Int. J. Nanomedicine 11 (2016) 6621–6634, http://dx.doi.org/10.2147/IJN.S113692.

[27] N.E.A. El-Naggar, M.H. Hussein, A.A. El-Sawah, Bio-fabrication of silver nanoparticles by phycocyanin, characterization, in vitro anticancer activity against breast cancer cell line and in vivo cytotxicity, Sci. Rep. 7 (2017) 10844, http://dx.doi.org/10.1038/s41598-017-11121-3.

[28] E. Zielinska, A. Zauszkiewicz-Pawlak, M. Wojcik, I. Inkielewicz-Stepniak, Silver nanoparticles of different sizes induce a mixed type of programmed cell death in human pancreatic ductal adenocarcinoma, Oncotarget 9 (4) (2018) 4675–4697, http://dx.doi.org/10.18632/oncotarget.22563.

[29] A.V. Karpukhin, N.V. Avkhacheva, R.Y. Yakovlev, I.I. Kulakova, V.A. Yashin, G.V. Lisichkin, V.G. Safronova, Effect of detonation nanodiamonds on phagocyte activity, Cell Biol. Int. 35 (2011) 727–733, http://dx.doi.org/10.1042/CBI20100548.

[30] O.S. Wolfbeis, An overview of nanoparticles commonly used in fluorescent bioimaging, Chem. Soc. Rev. 44 (2015) 4743–4768.

[31] R. Rajan, K. Chandran, S.L. Harper, S. Yun, P.T. Kalaichelvan, Plant extract synthesized silver nanoparticles: an ongoing source of novel biocompatible materials, Ind. Crop. Prod. 70 (2015) 356–373.

[32] N. Martins, I.C. Ferreira, L. Barros, S. Silva, M. Henriques, Candidiasis: predisposing factors, prevention, diagnosis and alternative treatment, Mycopathologia 177 (2014) 223–240.

[33] P.K. Mukherjee, B. Sendid, G. Hoarau, J.F. Colombel, D. Poulain, M.A. Ghannoum, Mycobiota in gastrointestinal diseases, Nat. Rev. Gastroenterol. Hepatol. 12 (2015) 77–87.

[34] Z. Yehuda, B. Saar, D. Estella, S. Vadim, I. Clariel, H. Tamar, Colonization of *Candida*: prevalence among tongue-pierced and non-pierced immunocompetent adults, Oral Dis. 16 (2010) 172–175.

[35] J.G. Tortora, J. Mibrobiology: An Introduction, Pearson, Benjamin Cummings, San Francisco, CA, 2010, p. 758.

[36] H.A. Khan, A. Ahmad, R. Mehboob, Nosocomial infections and their control strategies, Asian Pac. J. Trop. Biomed. 5 (2015) 509–514.

[37] S. Qayyum, M. Oves, A.U. Khan, Obliteration of bacterial growth and biofilm through ROS generation by facilely synthesized green silver nanoparticles, PLoS One 12 (2017) e0181363.

[38] M. Oves, M.S. Khan, Z. Almas, A.S. Ahmad, F. Ahmed, E. Ahmad, A. Sherwani, M. Owais, A. Azam, Antimicrobial and cytotoxic efficacy of extracellular silver nanoparticles biofabricated from chromium reducing novel OS4 strain of *Stenotrophomonas maltophila*, PLoS One 8 (2013) e59140.

[39] A.W. Bauer, D.M. Perry, W.M.M. Kirby, Single disc antibiotic sensitivity testing of *Staphylococci*, A.M.A. Arch. Intern. Med. 104 (1959) 208–216.

[40] L.Q. Chen, L. Fang, J. Ling, C.Z. Ding, B. Kang, C.Z. Huang, Nanotoxicity of silver nanoparticles to red blood cells: size dependent adsorption, uptake, and hemolytic activity, Chem. Res. Toxicol. 28 (2015) 501–509.

[41] J. van Meerloo, G.J.L. Kaspers, J. Cloos, Cell sensitivity assays: the MTT assay, Methods Mol. Biol. 1743 (2011) 237–245 (Humana Press).

[42] R.M. Ahmar, M. Owais, R. Rajpoot, F. Ahmad, N. Khan, S. Zubair, Biomimetically synthesized ZnO nanoparticles attain potent antibacterial activity against less susceptible *S. aureus* skin infection in experimental animals, RSC Adv. 7 (58) (2017) 36361–36373.

[43] S. Kasibhatla, G.P. Amarante-Mendes, D. Finucane, T. Brunner, E. Bossy-Wetzel, D.R. Green, Acridine orange/ethidium bromide (AO/EB) staining to detect apoptosis, Cold Spring Harb Protoc 2006 (3) (2006) (pdb-prot 4493).

[44] H. Hu, N.S. Ahn, X. Yang, Y.S. Lee, K.S. Kang, *Ganoderma lucidum* extract induces cell cycle arrest and apoptosis in MCF-7 human breast cancer cell, Int. J. Cancer 102 (3) (2002) 250–253.

[45] Y. Yin, M. Shen, Z. Tan, S. Yu, J. Liu, G. Jiang, Particle coating-dependent interaction of molecular weight fractionated natural organic matter: impacts on the aggregation of silver nanoparticles, Environ. Sci. Technol. 49 (2015) 6581–6589.

[46] B.J. Wiley, S.H. Im, Z.Y. Li, J. McLellan, A. Siekkinen, Y. Xia, Maneuvering the surface plasmon resonance of silver nanostructures through shape-controlled synthesis, J. Phys. Chem. B 110 (2006) 15666–15675.

[47] V.K. Sharma, K.M. Siskova, R. Zboril, J.L. Gardea-Torresdey, Organic-coated silver nanoparticles in biological and environmental conditions: fate, stability and toxicity, Adv. Colloid Interf. Sci. 204 (2014) 15–34.

[48] R.S. Yehia, H. Al-Sheikh, Biosynthesis, and characterization of silver nanoparticles produced by *Pleurotus ostreatus* and their anticandidal and anticancer activities, World J. Microbiol. Biotechnol. 30 (2014) 2797–2803.

[49] A. Ahmad, P. Mukherjee, S. Senapati, D. Mandal, M.I. Khan, R. Kumar, M. Sastry, Extracellular biosynthesis of silver nanoparticles using the fungus *Fusarium oxysporum*, Colloids Surf. B: Biointerfaces 28 (2003) 313–318.

[50] M. Khan, M. Khan, S.F. Adil, M.N. Tahir, W. Tremel, H.Z. Alkhathlan, M.R.Z. Siddiqui, Green synthesis of silver nanoparticles mediated by *Pulicaria glutinosa* extract, Int. J. Nanomedicine 8 (2013) 1507.

[51] J.B. Miller, J.M. Harris, E.K. Hobbie, Purifying Colloidal Nanoparticles through Ultracentrifugation with Implications for Interfaces and Materials, Langmuir 30 (2014) 7936–7946.

[52] A. Hahn, G. Brandes, P. Wagener, S. Barcikowski, Metal ion release kinetics from nanoparticle silicone composites, J. Control. Release 154 (2011) 164–170.

[53] J. Liu, R.H. Hurt, Ion release kinetics and particle persistence in aqueous nano-silver colloids, Environ. Sci. Technol. 44 (2010) 2169–2175.

[54] S. Basu, P. Maji, J. Ganguly, Rapid green synthesis of silver nanoparticles by aqueous extract of seeds of *Nyctanthes arbor-tristis*, Appl. Nanosci. 6 (2016) 1–5.

[55] S. Shankar, A. Rai, A. Ahmad, M. Sastry, Rapid synthesis of Au, Ag, and bimetallic Au core-Ag shell nanoparticles using Neem (*Azadirachta indica*) leaf broth, J. Colloid Interface Sci. 275 (2004) 496.

[56] J. Huang, Q. Li, D. Sun, Y. Lu, Y. Su, X. Yang, H. Wang, Y. Wang, W. Shao, N. He, J. Hong, C. Chen, Biosynthesis of silver and gold nanoparticles by novel sundried *Cinnamomum camphora* leaf, Nanotechnology 18 (2007) 104–105.

[57] B. Ankamwar, M. Chaudhary, M. Sastry, Gold Nanotriangles biologically synthesized using tamarind leaf extract and potential application in vapor sensing, Synth. React. Inorg., Met.-Org., Nano-Met. Chem. 35 (2005) 19.

[58] N.L. Pacioni, D. Claudio, Borsarelli, R. Valentina, A.V. Veglia, Synthetic routes for the preparation of silver nanoparticles a mechanistic perspective, in: E.I. Alarcon, et al. (Ed.), Silver Nanoparticle Applications, Engineering Materials, Springer International Publishing, Switzerland, 2015, , http://dx.doi.org/10.1007/978-3-319-11262-6_2.

[59] Q. Sun, X. Cai, J. Li, M. Zheng, Z. Chen, C.P. Yu, Green synthesis of silver nanoparticles using tea leaf extract and evaluation of their stability and antibacterial activity, Colloids Surf. A Physicochem. Eng. Asp. 444 (2014) 226–231.

[60] H.E. Swanson, E. Tatge, Standard X-ray diffraction powder patterns. Vol. I, data for 54 inorganic substances, National Bureau of Standards, Washington, D.C. LT. B. S. Circular. 539, 1953, pp. 1–21.

[61] I.A. Wani, A. Ganguly, J. Ahmed, T. Ahmad, Silver nanoparticles: ultrasonic wave assisted synthesis, optical characterization and surface area studies, Mater. Lett. 65 (2011) 520–522.

[62] A. Becheri, M. Durr, P.L. Nostro, P. Baglioni, Synthesis and characterization of zinc oxide nanoparticles: application to textiles as UV-absorbers, J. Nanopart. Res. 10 (2008) 679–689.

[63] G.A. Kahrilas, W. Haggren, R.L. Read, L.M. Wally, S.J. Fredrick, M. Hiskey, J.E. Owens, Investigation of antibacterial activity by silver nanoparticles prepared by microwave-assisted green syntheses with soluble starch, dextrose, and arabinose, ACS Sustain. Chem. Eng. 2 (2014) 590–598.

[64] N.A. Amro, L.P. Kotra, K.W. Mesthrige, A. Bulychev, S. Mobashery, G.Y. Liu, High-resolution atomic force microscopy studies of the *Escherichia coli* outer membrane: structural basis for permeability, Langmuir 16 (2000) 2789–2796.

[65] D.R. Monteiro, A.S. Takamiya, L.P. Feresin, L. Fernando, E.R. deCamargo, A.C.B. Delbem, M. Henriques, D.B. Barbosa, Susceptibility of *Candida albicans* and *Candida glabrata* biofilms to silver nanoparticles in intermediate and mature development phases, J. Prosthodont. Res. 59 (2015) 42–48.

[66] H.M.M. Ibrahim, Green synthesis, and characterization of silver nanoparticles using banana peel extract and their antimicrobial activity against representative microorganisms, J. Radiat. Res. Appl. Sci. 59 (2015) 42–48.

[67] N.R. Jabir, K. Anwar, C.K. Firoz, M. Oves, M.A. Kamal, S. Tabrez, An overview on the current status of cancer nanomedicines, Curr. Med. Res. Opin. (2018), http://dx.doi.org/10.1080/03007995.2017.1421528 (in press).

[68] Z.W. Huang, T.T. Ding, J. Sun, Study of effect on cell proliferation and hemolysis of HAP and TCP nanometer particles, Adv. Mater. Res. 378 (2012) 711–714.

[69] H. Wei, T. Ding, J. Sun, D. Xu, Preliminary Study of Biological Evaluation on

Hydroxyapatite Nanoparticles, (2010), pp. 1425–1426.
[70] T. Mocan, Hemolysis as expression of nanoparticles-induced cytotoxicity in red blood cells, Biotechnol. Mol. Biol. Nanomed. 1 (2013) 1.
[71] J. Choi, V. Reipa, V.M. Hitchins, P.L. Goering, R.A. Malinauskas, Physicochemical characterization and in vitro hemolysis evaluation of silver nanoparticles, Toxicol. Sci. 123 (2011) 133–143.
[72] J.M. Zook, R.I. MacCuspie, L.E. Locascio, M.D. Halter, J.T. Elliott, Stable nanoparticle aggregates/agglomerates of different sizes and the effect of their size on hemolytic cytotoxicity, Nanotoxicology (2011) 1–14.
[73] P. Devaraj, P. Kumari, C. Aarti, A. Renganathan, Synthesis and characterization of silver nanoparticles using cannonball leaves and their cytotoxic activity against MCF-7 cell line, J. Nanotechnol. 13 (2013) (598328-5).
[74] A.H.A. Kelkawi, A.A. Kajani, A.K. Bordbar, Green synthesis of silver nanoparticles using *Mentha pulegium* and investigation of their antibacterial, antifungal and anticancer activity, IET Nanobiotechnol. 11 (2017) 370–376, http://dx.doi.org/10.1049/iet-nbt.2016.0103.
[75] M.A. Farah, M.A. Ali, S.M. Chen, Y. Li, F.M. Al-Hemaid, F.M. Abou-Tarboush, K.M. Al-Anazi, J. Lee, Silver nanoparticles synthesized from *Adenium obesum* leaf extract induced DNA damage, apoptosis and autophagy via generation of reactive oxygen species, Colloids Surf. B: Biointerfaces 141 (2016) 158–169, http://dx.doi.org/10.1016/j.colsurfb.2016.01.027.
[76] Y. Pan, S. Neuss, A. Leifert, M. Fischler, F. Wen, U. Simon, G. Schmid, W. Brandau, W. Jahnen-Dechent, The apoptotic effect of nanosilver is mediated by a ROS- and JNK-dependent mechanisminvolving the mitochondrial pathway in NIH3T3 cells, Small 3 (2007) 1941–1949.
[77] Y.H. Hsin, C.F. Chen, S. Huang, T.S. Shih, P.S. Lai, P.J. Chueh, The apoptotic effect of nanosilver is mediated by a ROS- and JNK-dependent mechanism involving the mitochondrial pathway in NIH3T3 cells, Toxicol. Lett. 179 (2008) 130–139.
[78] S.A. Loutfy, N.A. Al-Ansary, N.T. Abdel-Ghani, A.R. Hamed, M.B. Mohamed, J.D. Craik, T.A. Eldin, A.M. Abdellah, Y. Hussein, M.T. Hasanin, S.E. Elbehairi, Antiproliferative activities of metallic nanoparticles in an in vitro breast cancer model, Asian Pac. J. Cancer Prev. 16 (2015) 6039–6046.